

# Analytical modeling of large-angle CMBR anisotropies from textures

J.C.R. Magueijo

Mullard Radio Astronomy Observatory, Cavendish Laboratory  
Madingley Road  
Cambridge, CB3 0HE, UK

and

Department of Applied Mathematics and Theoretical Physics  
University of Cambridge  
Cambridge CB3 9EW, UK.

## Abstract

We propose an analytic method for predicting the large angle CMBR temperature fluctuations induced by model textures. The model makes use of only a small number of phenomenological parameters which ought to be measured from simple simulations. We derive semi-analytically the  $C^l$ -spectrum for  $2 \leq l \leq 30$  together with its associated non-Gaussian cosmic variance error bars. A slightly tilted spectrum with an extra suppression at low  $l$  is found, and we investigate the dependence of the tilt on the parameters of the model. We also produce a prediction for the two point correlation function. We find a high level of cosmic confusion between texture scenarios and standard inflationary theories in any of these quantities. However, we discover that a distinctive non-Gaussian signal ought to be expected at low  $l$ , reflecting the prominent effect of the last texture in these multipoles.

MRAO/1782  
DAMTP/94-101

# 1 Introduction

In the recent past, a large amount of work has been directed towards predicting the CMBR temperature anisotropies associated with inflationary scenarios (see [1] for a review), and with the various topological defect scenarios (e.g. [2, 3]). Inflationary scenarios are far better explored in this respect. The main reason for this is that it is easier in these models to plead ignorance of the detailed mechanism responsible for the density fluctuations of the Universe. Quantum fluctuations in the metric are a fuzzy subject, and hand-waving arguments for Gaussian fluctuations with a particular type of spectrum are normally considered acceptable. Once this is done, one is free to take advantage of the well developed and sophisticated industry of methods aimed at treating Gaussian fluctuations [4]. A precise prediction for the outcome of concrete experiments follows easily, making inflation popular with experimentalists. The state of affairs in topological defect scenarios is rather different. No lack of fundamental physics understanding hampers working out in rigour the defect network evolution and the fluctuations they induce on the matter and radiation of the Universe. The price to pay for our honesty is that a serious treatment of the problem is computationally overpowering. A reliable link between the defect network and the perturbations it induces is undoubtedly still missing. To top off the trouble, it turns out that the fluctuations induced by defects are often non-Gaussian. Setting up a data-analysis framework geared towards non-Gaussian fluctuations is virgin ground (but see [4, 5, 6, 7] for Gaussianity tests). Overall, even though defect scenarios have so far been poor in solid predictions, they have a potentially polemic value not to be discarded. Non-Gaussian data analysis does not exist partly because non-Gaussian theories are too vast a class to be treated in one go. Defect scenarios provide a motivated and topical example with which one can rehearse non-Gaussian data analysis techniques and experimental strategies.

The main technical complication in predicting CMBR fluctuations in defect scenarios arises from the fact that  $\frac{\delta T}{T}$  maps photograph the whole sky (that is, our past light cone clipped by the last scattering surface) and not just its intersection with the last scattering surface. Hence the defect network, surrounding matter, and CMBR photons have to be evolved through a large number of expansion times. The problem is usually tackled by means of full-blown simulations [2, 3]. These require access to supercomputers, and even so face severe limitations. Important issues like cosmic variance in defect scenarios have hardly been addressed. A possible computational short cut can be found if one is to assume scaling. The defects network is expected to scale, by which one means that it looks statistically the same at any time, once the network length scale is equated to the horizon distance. This suggests dividing the sky cone into cells corresponding to expansion times and horizon volumes. Scaling makes it plausible that the CMBR pattern in each of these cells is statistically the same, once some angular scaling procedure is applied to it. This being the case, all that is required from the sim-

ulations is good statistics for the CMBR spots induced by defects inside horizon size boxes during one expansion time. Such simulations are considerably easier to perform. A prototype of this type of study is [8]. In the case of textures, the short-cut which we have described has been adopted by [9] where a “scaling-spot-throwing” process was implemented on a computer. The spots were all derived from model SSSS (self-similar and spherically symmetric) collapses. In this paper we advocate the use of analytical techniques for scaling-spot-throwing. An analytical approach allows the derivation of exact formulae for the  $C^l$ ,  $C(\theta)$ , and their cosmic variance, from which interesting general properties can be derived. These properties are naturally less evident in computer simulations, unless one explicitly sets out to find them. Furthermore, an analytical approach allows the treatment of a more general case than [9]. The method proposed here applies to quasi-circular spots with any profile. The scaling size ( $p_s$ ), number density ( $n$ ), and brightness factor ( $a$ ) of the spots are also left as free parameters. We should admit that only the brightness factor is a truly free parameter in the texture model. All others should be considered as phenomenological in origin, eventually to be fixed by simulations. As they still constitute a controversial matter, we choose to consider a broader class of model spots. We can then sort out which spot properties it is really important to measure from the simulations.

The plan of this paper is as follows. In Sec.2 we start by deriving the statistical properties of scaling texture model collapses as they appear in the sky cone, and from these a formal solution for the joint distribution function of the CMBR  $a_m^l$  is given. Using this solution, in Secs.3.1 and 3.3 we derive exact formulae for the  $C^l$  and  $\sigma(C_l)$  in texture models. We prove the general result that the cosmic variance in the  $C_l$  is larger in texture scenarios than in Gaussian theories. The excess variance is negligible for high  $l$ , but significant at low  $l$ . In Secs.3.2 and 3.4 we compute numerically the  $C^l$  spectra (with cosmic variance error bars) for a large class of spot types. We find that the spots’ profile, intensity, and number density affect only the spectrum normalization. The spectrum shape is largely controlled by the spots’ scaling size  $p_s$  alone. In general, the spectra are slightly tilted (and we numerically compute the dependence of the tilt on  $p_s$ ), but with an extra suppression of power at low  $l$ . In Sec.4 we derive expressions for the two-point correlation function  $C(\theta)$  and its cosmic variance. Although closer to experiment,  $C(\theta)$  appears to be a very bad discriminator between texture and inflationary scenarios. The most original result proved in this paper is presented in Sec.5, where we ask how many textures are responsible for a given  $a_m^l$ . For high  $l$ , this number goes like  $l$ , suggesting Gaussian behaviour. For low  $l$  we find that the  $a_m^l$  are mostly due to the effects of a single texture: the last (that is, the closest) texture. This ought to impart a peculiar non-Gaussian signal to the low  $a_m^l$ , a fact which we prove explicitly. The purpose of the sequel to this paper [10] is to devise a low- $l$  data-analysis technique (in the moulds of [11]) capable of fully characterising this effect.

## 2 Analytical spot-throwing

In topological defect scenarios the CMBR fluctuations at large angles are due only to the ISW (integrated Sachs-Wolfe) effect caused by the defect network ([2]). For a standard recombination scenario the validity range for this approximation is  $2 \leq l \leq 30$ . If early reionization occurs, the upper limit for this range becomes the value of  $l$  corresponding to the angular scale of the horizon at “last scattering” (defined in some conservative way). As it is not clear which is the most sensible scenario we take as a working hypothesis the choice which maximizes the applicability of our model: standard recombination. Now if we assume that the statistical scaling of the texture fields extends to their associated time-dependent metric perturbations, then we may expect the ISW spots themselves to scale. This allows the direct modelling of the statistics for texture induced spots as they appear in the sky. From these, we can then write an expression for the  $a_m^l$  joint distribution function for  $2 \leq l \leq 30$ . For simplicity, we will assume that the texture spots are independent (not required by the formalism, but a good approximation). Then each texture angular position in the sky is uniformly distributed. Furthermore its time position in the sky cone can be associated with a modified Poisson process in time, in which the probability of an event is allowed to vary. Let  $n$  be the average number of texture spot producing configurations per horizon volume. Then their average volume density is

$$\rho = \frac{2n}{9\pi t^3} \quad (1)$$

and using the relation between the proper area  $dS$ , the time of emission  $t$ , and the apparent solid angle  $d\Omega$ :

$$dS = d\Omega \left( 3t \left( \left( \frac{t_0}{t} \right)^{1/3} - 1 \right) \right)^2 \quad (2)$$

we find that the angular density of spots in the sky per unit of emission time is

$$\delta(t) = \frac{2n}{\pi t} \left( \left( \frac{t_0}{t} \right)^{1/3} - 1 \right)^2. \quad (3)$$

It is convenient to introduce the variable  $y = \log_2(t_0/t)$ , the expansion time number as we go backwards in time. Each  $\Delta y = 1$  represents one expansion time, starting from  $y_0 = 0$  (here and now) and going as far as  $y_{l_s} = \log_2(t_0/t_{l_s})$ , when we hit the last scattering surface. In the standard recombination scenario  $y_{l_s} \approx 15$ . In terms of  $y$  the spot density in the sky is

$$N(y) = 2n \log(2) \left( 2^{y/3} - 1 \right)^2. \quad (4)$$

Let us now introduce a Poisson-type process in  $y$ , with a variable probability density  $N(y)$ . If  $p_n(y)$  is the probability of having exactly  $n$  textures at  $y' < y$ , then

$$\frac{dp_n}{dy} = N(y)(p_{n-1} - p_n) \quad , \quad p_{-1} = 0 . \quad (5)$$

This hierarchy of equations fully specifies the statistics of the textures' time-position in the sky. From the  $p_n(y)$  one can also derive the probability density of the  $n^{\text{th}}$  texture position  $y_n$  by means of

$$P_n(y_n) = p_{n-1}(y_n)N(y_n) . \quad (6)$$

However one should be wary of the  $y_n$  variables, as they are not independent. Not only are their ranges constrained by  $y_1 < y_2 < \dots < y_n$  but also their statistical dependence is patent in the conditional distribution functions. From (5) and (6) one has that

$$P_1(y_1) = N(y_1)e^{-\int_0^{y_1} dy N(y)} \quad (7)$$

but then

$$P_2(y_2|y_1) = N(y_2)e^{-\int_{y_1}^{y_2} dy N(y)} \quad (8)$$

which is dependent on  $y_1$ . From these expressions we can derive the joint distribution function

$$P_{12}(y_1, y_2) = N(y_1)N(y_2)e^{-\int_0^{y_2} dy N(y)} \quad (9)$$

which misleadingly factorizes. More generally one has

$$P_{1\dots n}(y_1, y_2, \dots, y_n) = N(y_1)N(y_2)\dots N(y_n)e^{-\int_0^{y_n} dy N(y)} . \quad (10)$$

The statistics contained in  $P_n$  or  $p_n$  refer to a sequence of textures ordered in  $y$ . Ordering will be crucial in Section 5 when we uncover the last texture. However for some other purposes (like the derivations in Section 3) we may simply consider unordered textures. Then we have a total of  $N_t = \int_0^{y_t} dy N(y) \gg 1$  textures in the sky. Their positions  $y_n$  are independent random variables with a distribution

$$P_n(y_n) = \frac{N(y_n)}{N_t} \quad (11)$$

for all  $n$ , which is considerably simpler.

We now model the texture spot patterns. These ought to follow some sort of statistical scaling law, where the scale angle is

$$\theta^s(y) = \arcsin \left( \min \left( 1, \frac{p_s}{2y/3 - 1} \right) \right) \quad (12)$$

for a pattern laid at time  $y$ . Here  $p_s$  is the scaled impact parameter ( $p_s = p/(3t)$ ) giving  $\sigma_s = \pi p_s^2$ , the scaled cross section for photon anisotropies. Causality requires that  $p_s < 1/2$ . It may happen that  $p_s$  is a random variable itself, but

we shall ignore this complication. For small, nearly circular spots with profile  $W^s(\theta, y)$ , scaling implies that

$$W^s(\theta, y) = \overline{W}(x) \quad (13)$$

with  $x = \theta/\theta^s$ . This is a sensible scaling law even for  $y < 1$ , although for  $y < 1$  the exact scaling law should be more complicated, as the photons propagating through the scaling metric no longer move along parallel trajectories. In particular, if  $y < y_0 = 3 \log(1 + p_s)$ , we live inside a texture and are enclosed by its pattern. Unless  $(2np_s)^3 \approx 1$  textures like these are very rare, and the approximation (13) should produce good enough final results.

We seek to write the  $a_m^l$  coefficients for skies filled with nearly circular spots described by the above statistics. For each of these spots let us first point the  $z$ -axis at their centre, and perform the spherical harmonic decomposition in that frame. We obtain an expression of the form

$$\tilde{a}_m^l(n) = a_n W^{sl}(y_n) \cdot \sqrt{\frac{2l+1}{4\pi}} \cdot \delta_{m0} + \epsilon_m^l \quad (14)$$

where  $W^{sl}$  is the Legendre transform of the scaled profile:

$$W^{sl} = 2\pi \int_{-1}^1 dz P^l(z) W^s(z, y_n) \quad (15)$$

and  $\epsilon_m^l$  is a perturbation induced by the eccentricity. This perturbation is negligible, even if the spots are not very nearly circular, but  $l \ll [1/\theta^s(y_n)]$ . The extra factor  $a_n$  in (15) accounts for the texture brightness, and is a random variable with a  $y_n$ -independent distribution function. Performing a rotation to a general frame, where the  $n^{\text{th}}$  texture has coordinates  $\Omega_n$ , and summing over all textures one finally obtains:

$$a_m^l = \sum_n a_n W^{sl}(y_n) Y_m^{l*}(\Omega_n) . \quad (16)$$

The variables  $a_n$  are independent but equally distributed. Their distribution has to be determined from the simulations. The  $\Omega_n$  are uniformly distributed, and from them one can determine the  $Y_m^l(\Omega_n)$  distributions (but with care, as the  $Y_m^l$  are not independent). Finally from (10), (12), and (15) one can determine the  $W_n^{sl}$  distributions. The  $W_n^{sl}$  makes the various terms in (16) dependent variables, rendering an analytic approach for the  $a_m^l$  distributions through (16) unfeasible. In any case finding the marginal distributions of the  $a_m^l$  would not be the end of the story, since the  $a_m^l$  are necessarily dependent random variables (see [11]). Hence we still would have to find the joint distribution  $F(a_{m_1}^{l_1}, a_{m_2}^{l_2}, \dots)$  for a complete solution to the problem of cosmic variance in texture scenarios. Expression (16) constitutes a formal solution to this problem which, despite all the obstacles to an analytical solution, is particularly suited to Monte Carlo simulations. It

separates the individual effect of each texture on each of the  $a_m^l$ . It also factorizes each texture contribution into three factors. The  $Y_m^{l\star}$  are purely geometrical factors which should be present in any SSS (statistically spherically symmetric) theory (see [11] for a definition). The  $W_n^{sl}$  are a reflection of the structure of the sky (foliation into expansion times and horizon volumes) and should be present whenever there is scaling. Finally, the  $a_n$ 's factor out all that is peculiar to the texture model under consideration, and will have to be measured from detailed texture simulations.

### 3 The angular power spectrum

#### 3.1 An expression for the $C^l$

Throughout this paper we will use the notation  $C_l$  for the angular power spectrum of realizations, and  $C^l$  for its ensemble average. Whereas  $C_l$  is a random variable,  $C^l$  is a number. In any SSS theory one has

$$\langle a_m^l a_{m'}^{l\star} \rangle_{obs} = C^l \delta_l^m \delta_{m'}^l . \quad (17)$$

The  $C^l$  can be estimated from the observable

$$C_l = \frac{1}{2l+1} \sum_{m=-l}^l |a_m^l|^2 \quad (18)$$

since  $\langle C_l \rangle_{obs} = C^l$  in any SSS theory. Cosmic variance introduces error bars of size  $\sigma(C_l)$  into this estimate. We start by deriving an exact expression for the  $C^l$ . From (16) and (18) we have that

$$C^l = \langle C_l \rangle = \frac{1}{2l+1} \sum_m \sum_{nn'} \langle a_n a_{n'} \rangle \langle W_n^l W_{n'}^l \rangle \langle Y_m^{l\star}(\Omega_n) Y_m^l(\Omega_{n'}) \rangle \quad (19)$$

but since

$$\langle Y_m^{l\star}(\Omega_n) Y_m^l(\Omega_{n'}) \rangle_{obs} = \frac{\delta_{nn'}}{4\pi} \quad (20)$$

we have simply

$$C^l = \frac{\langle a^2 \rangle}{4\pi} \sum_n \langle W_n^{l2} \rangle . \quad (21)$$

Computing the averages using the unordered statistical description (11) we can write

$$C^l = \frac{\langle a^2 \rangle}{4\pi} \int_0^{y_{ls}} dy N(y) W^{ls2}(y) . \quad (22)$$

If  $p_s$  is a random variable with distribution  $f(p_s)$ , then expression (22) still holds but now with  $W^{sl2}$  replaced by  $\int dp_s f(p_s) W^{sl2}(y, p_s)$ . Expression (22) lends itself to be written as

$$C^l = \int_0^{y_{ls}} dy C^l(y) \quad (23)$$

Missing author supplied figuresMissing author supplied figures

Figure 1: The density  $C^l(y)$  multiplied by  $l(l+1)$  for  $l$  from 2 to 30 for  $(n = 1, p_s = 0.4)$  and  $(n = 1, p_s = 0.08)$  textures with Gaussian profile spots.

thus defining a density

$$C^l(y) = \frac{\langle a^2 \rangle}{4\pi} N(y) W^{ls^2}(y) \quad (24)$$

measuring the contribution of textures living at time  $y$  to a given  $C^l$ . In Fig. 1 we have plotted  $l(l+1)C^l(y)$  for  $(n = 1, p_s = 0.4)$  and  $(n = 1, p_s = 0.08)$  textures with Gaussian profile spots, for  $l$  from 2 to 30. These plots are to be confronted with the common belief that a given  $C^l$  is mostly due to textures living at a time when the apparent size of the horizon equals the multipole angular scale. We find instead that  $C^l(y)$  peaks for  $y: \Omega^s(y) \approx \frac{4\pi}{l(l+1)}$ , that is, when the textures' apparent size fits the multipole angular scale. Furthermore the peaks comprise several generations and an accurate prediction for the  $C^l$  spectrum can never neglect any of the integrand in (23). Changing  $n$  only affects the normalization of  $C^l(y)$ . Reducing  $p_s$  not only decreases the normalization but also shifts the peaks to the left necessarily affecting the shape of the integrated  $C^l$ . In general as  $l$  increases the peak's heights (multiplied by  $l(l+1)$ ) are slightly reduced, but their width increases. The delicate balance of these two effects will determine whether the  $C^l$  spectrum is flat or not.

### 3.2 Profiles and reduced $a$ and $p_s$

It is not clear what profile  $\overline{W}$  real texture spots have. Simulations [2, 8] suggest that the well-known SSSS profile may be oversimplified. We find that the exact profile form has little impact on the  $C^l$ -spectra. For intermediate  $l$ , profiles do not matter at all, and for low  $l$  they induce differences easily confused by cosmic variance. The issue of matching free parameters for different profiles is, however, non-trivial. We have considered the following profiles:

1.-**Hat profile.** Defined by

$$\overline{W}^s(x) = H(1 - x) \quad (25)$$

where  $H$  is the Heaviside function. Its Legendre transform is

$$W^{sl} = 2\pi \int_{\cos \theta^s}^1 dz P^l(z) = \frac{2\pi}{2l+1} (P_{l+1}(\cos \theta^s) - P_{l-1}(\cos \theta^s)), \quad (26)$$

the  $l$ -weighted scaled solid angle.



**2.-Toy hat profile.** We can skip the complications induced by the Legendre polynomials approximating the hat profile by

$$W^{sl2} = \begin{cases} \Omega^{s2} & \text{for } \Omega^s < \Omega^{l(sat)} = \frac{4\pi}{l(l+1)} \\ \Omega^{l(sat)2} & \text{for } \Omega^s > \Omega^{l(sat)} \end{cases} \quad (27)$$

with

$$\Omega^s = 2\pi(1 - \cos \theta^s) . \quad (28)$$

the scaled solid angle.

**3.-Gaussian profile.** A large angle generalization of the well-known small angle Gaussian window:

$$W^{ls} = \Omega^s e^{-\frac{(l+\frac{1}{2})^2 \theta^{s2}}{2}} . \quad (29)$$

**4.-SSSS profile.** A profile of the form (e.g. [12])

$$W^s(\theta, y) \propto \frac{\theta^s}{\sqrt{2\theta^{s2} + \theta^2}} \quad (30)$$

with some sort of cut off at

$$\theta^h(y) = \arcsin \left( \min \left( 1, \frac{1/2}{2y/3 - 1} \right) \right) \quad (31)$$

the angle subtended by the horizon. We define this cut off with the Legendre transform:

$$W^{sl} = \begin{cases} 2\pi\theta^h\theta^s e^{-\sqrt{2}\theta^s/\theta^h} & \text{for } l \leq [1/\theta^h] \\ 2\pi\theta^s \frac{e^{-\sqrt{2}\theta^s l}}{l} & \text{for } l \geq [1/\theta^h] . \end{cases} \quad (32)$$

The hat profile is suggested by the belief that  $\frac{\delta T}{T}$  circular averages are all that matters for  $2 \leq l \leq 30$ . Circular averages have been extensively studied (eg. [13]) and some useful properties have been found for them. The toy hat profile, due to its simplicity, is ideal for an heuristic explanation of the results obtained (Sec.3.5). The Gaussian profile is particularly amenable to analytical work, thus providing a good check on the numerics. Furthermore it is probably a good approximation to the peaks found in [8]. Finally, there is no harm in considering the SSSS profile, for it might have something to do with reality after all.

With the  $\overline{W}$  defined as they are, the functions  $C^l(y)$  peak for different values of  $y$ . To facilitate comparison we should therefore define a reduced  $p_s$ :

$$\overline{p}_s = \frac{p^{hat}}{1.8} = \frac{p^{toy}}{2} = p^{gauss} \quad (33)$$

which ensures that, for high  $l$ ,  $C^l(y)$  peaks at the same  $y_{max}$  for the same  $\overline{p}_s$  for all profiles. For the SSSS profile  $C^l(y)$  peaks always for  $y : \theta^h(y) \approx \frac{1}{l}$ . This is

## Missing author supplied figures

Figure 2:  $C^{20}(y)$  for the hat profile (oscillating line), the toy hat profile (non-oscillating line), and Gaussian profile (with points). For all the curves  $\bar{p}_s = 0.2$  and  $\langle \bar{a}^2 \rangle$  is the same.

understandable as the integrated anisotropy increases logarithmically as we go away from the core. As a result, the effective cross-section for SSSS textures is the horizon area, for all  $p_s$ . For this reason we will always treat the SSSS profile separately, as it does not really have a parameter  $p_s$ .

It also happens that the value of  $C^l(y_{max})$  depends on the profile, taking the form

$$C^l(y_{max}) = \frac{\langle a^2 \rangle \cdot 2n \log(2) \cdot \pi p_s^2}{l(l+1)} \cdot \alpha \quad (34)$$

with  $\alpha^{hat} \approx 0.58$ ,  $\alpha^{toy} = 1$ ,  $\alpha^{gauss} = 1/(4e)$ . By defining a reduced  $a$  as

$$\bar{a} = a \sqrt{\alpha \frac{p_s}{\bar{p}_s}} = 1.05 a^{hat} = 2 a^{toy} = \frac{a^{gauss}}{2\sqrt{e}} \quad (35)$$

we can ensure that  $C^l(y_{max})$  for high  $l$  is the same for all the profiles with the same  $\langle \bar{a}^2 \rangle$  and  $\bar{p}_s$ .

In Fig. 2 we have plotted  $C^{20}(y)$  in units of  $\langle \bar{a}^2 \rangle n$ , with  $\bar{p}_s = 0.2$ , for the first three profiles proposed. We notice that for  $y > y_{max}$  all the  $C^l(y)$  have the same form, as for all profiles  $W^{ls} \propto \Omega^s$  (even though the proportionality constants may be different). Consequently, in this region  $C^l(y) \propto \Omega^s(y) \propto 1/N(y)$  regardless of the profile. For  $y \ll y_{max}$  we have  $W^{ls} \ll \Omega^s$  and so  $C^l(y)$  is proportional to  $N(y)$  or smaller than that. The exact form of  $C^l(y)$  in this region is profile dependent, as it involves details of how  $W^{ls}(\Omega^s)$  starts to cut off at a particular scale. While this portion of the integrand is not the main contribution to the total  $C^l$  it is clear that the detailed form of the spectrum is going to be profile dependent. It remains to be seen if these differences have any meaning once cosmic variance error bars are taken into account.

It is also in the  $y \ll y_{max}$  region that  $C^l(y)$  may be affected by the existence of non-spherical spot modes ( $\epsilon_m^l$  in (14)). These are the only source of inaccuracies in the model proposed, and so whatever mistakes we make will be in this region. Like profile differences, spots' ellipticity can only affect the final  $C^l$  in the fine detail. Most probably, ellipticity affects  $C^l$  even less than the profile, as the spots seen in the simulations appear to be very circular.

### 3.3 An expression for $\sigma^2(C_l)$

We now turn to the issue of cosmic variance in the  $C_l$ . This turns out to depend on the nature of the theory. It is known that in Gaussian theories the  $C_l$  are

### Missing author supplied figures

Figure 3: The relative non-Gaussian excess variance  $\tilde{\epsilon}^l(p_s)$  for Gaussian profile spots.

$\chi_{2l+1}^2$ -distributed with a variance

$$\sigma_G^2(C_l) = C^{l2} \frac{2}{2l+1}. \quad (36)$$

In some of the literature these are also the cosmic variance error bars attributed to non-Gaussian theories. We will use our model to compute directly  $\sigma_{TX}^2(C_l)$ . From (16) we have that

$$\begin{aligned} \langle C_l^2 \rangle_{obs} &= \frac{1}{(2l+1)^2} \sum_{mm'} \sum_{(n_1 n_2 n_3 n_4)} \langle a_{n_1} a_{n_2} a_{n_3} a_{n_4} \rangle \langle W_{n_1}^l W_{n_2}^l W_{n_3}^l W_{n_4}^l \rangle \\ &\quad \langle Y_m^{l*}(\Omega_{n_1}) Y_m^l(\Omega_{n_2}) Y_{m'}^{l*}(\Omega_{n_3}) Y_{m'}^l(\Omega_{n_4}) \rangle. \end{aligned} \quad (37)$$

The last factor can only be non-zero in one of the following cases:

- if  $n_1 = n_2$  and  $n_3 = n_4$  but  $n_1 \neq n_3$ , giving rise to  $(2l+1)^2$  terms,
- if  $n_1 = n_3$  and  $n_2 = n_4$  (but  $n_1 \neq n_2$ ) or  $n_1 = n_4$  and  $n_2 = n_3$  (but  $n_1 \neq n_2$ ), giving rise to a total of  $2(2l+1)$  terms,
- if  $n_1 = n_2 = n_3 = n_4$ , giving rise to a single term.

Putting all these terms together one has

$$\langle C_l^2 \rangle_{obs} = \frac{\langle a^2 \rangle^2}{(4\pi)^2} \sum_{n \neq n'} \langle W_n^{l2} W_{n'}^{l2} \rangle \left( 1 + \frac{2}{2l+1} \right) + \frac{\langle a^4 \rangle}{(4\pi)^2} \sum_n \langle W_n^{l4} \rangle. \quad (38)$$

Subtracting off  $C^{l2}$  written as (21), using (11), and neglecting terms in  $1/N_t$ , one finds after some algebra

$$\sigma_{TX}^2(C_l) = C^{l2} \left( \frac{2}{2l+1} + \left( 1 + \frac{\sigma^2(a^2)}{\langle a^2 \rangle^2} \right) \frac{\int_0^{y_{ls}} dy N(y) W^{ls4}(y)}{\left( \int_0^{y_{ls}} dy N(y) W^{ls2}(y) \right)^2} \right). \quad (39)$$

We note that the cosmic variance in the  $C^l$  in texture scenarios is always larger than in Gaussian theories. We define  $\epsilon^l$ , the relative size of the excess variance, as

$$\epsilon^l = \frac{\sigma_{TX}^2(C_l) - \sigma_G^2(C_l)}{\sigma_G^2(C_l)}. \quad (40)$$

Missing author supplied figures Missing author supplied figures Missing  
author supplied figures

Figure 4:  $C^{l\star}$  spectra for the hat, toy hat, and Gaussian profiles.

$\epsilon^l$  is a function of  $n$ ,  $p_s$ , and the profile. In general  $\epsilon^l(n, p_s) = \epsilon^l(1, p_s)/n$ , so we define  $\tilde{\epsilon}^l(p_s) = \epsilon^l(1, p_s)$ , the excess variance per unit of  $1/n$ . The quantity  $\epsilon^l$  can be seen as a (theoretical) indicator of how non-Gaussian a given multipole is. A texture theory with  $n \rightarrow \infty$  will be a Gaussian theory. A low  $n$  theory will be very non-Gaussian, at least for some  $l$ . In Fig. 3 we have plotted  $\tilde{\epsilon}^l(p_s)$  for spots with a Gaussian profile. Generally the excess variance is very small for high  $l < 30$ . For low  $l$  (say from 2 to 5) the correction can be considerable, the more so the smaller the  $p_s$ .

### 3.4 $C^{l\star}$ -spectra for different $\bar{p}_s$ and profiles

From (24) we see that the parameters  $\langle a^2 \rangle$  and  $n$  can only affect the overall normalization of the spectrum. Also (34) suggests that the ‘‘average’’ spectrum normalization is proportional to  $\pi p_s^2$ , although  $p_s$  may affect the spectrum shape as well. Furthermore a roughly scale invariant ( $\propto 1/l^2$ ) spectrum can be expected. We do want more than a rough prediction, though, so we define a reduced spectrum

$$C^{l\star} = \frac{4\pi l(l+1)C^l}{\langle \bar{a}^2 \rangle \cdot 2n \log(2) \cdot \pi \bar{p}_s^2}. \quad (41)$$

$C^{l\star}$  describes in detail departures from scale invariance and factors out all that contributes only to the normalization of the spectrum. It depends only on the profile and  $\bar{p}_s$ . In Fig. 4 we have plotted the  $C^{l\star}$  spectrum for various values of  $\bar{p}_s \leq 1/4$  (to ensure causality), for the hat, toy hat, and Gaussian profiles. The spectrum normalization still depends on the profile. Even though the peak heights in  $C^l(y)$  have been matched by our definitions of  $\bar{p}_s$  and  $\bar{a}$ , the differences in the peak’s shapes and in  $C^l(y)$  away from the peak produce different integrated  $C^l$  for different profiles. Apart from this it is remarkable that the  $C^{l\star}(\bar{p}_s)$  spectra shapes do not depend on the profile in any significant way. For intermediate scales ( $l_1 < l < 30$ , for some  $l_1$ ), the spectra are scale-invariant if  $\bar{p}_s$  is not too small. If  $\bar{p}_s$  is small, the spectrum is slightly tilted. Whatever the case, for low  $l$  ( $l < l_1$ ) the power is suppressed relative to a scale invariant (or slightly tilted) spectrum. An exact evaluation of the tilt,  $l_1$ , and low  $l$  suppression factor can only be done numerically. An approximate formula and heuristic explanation of this effect is given in Sec.3.5.

Missing author supplied figures

Figure 5:  $C^{l\star}$  spectrum (middle line) and its Gaussian (lines) and non-Gaussian (bars) cosmic variance error bars for spots with a SSSS profile with  $n=0.25$  and  $p_s = 0.2$ .

Missing author supplied figures

Figure 6: The spectral index  $n^i$  for high  $l$  as a function of  $\bar{p}_s$ .

### 3.4.1 SSSS collapses

We have applied our formalism to concrete choices of  $(n, \bar{p}_s)$  and profile which have often been suggested by simulations. In [9] there is the suggestion that it is a good approximation to consider that only SSSS collapses followed by unwindings cause CMBR spots. This leads to a scenario with a low spot number density ( $n \approx 0.25$ ), and regardless of  $p_s$  (which is a random variable in this case), to an effective spot size of the order of the horizon angular size. We have pointed out before that  $n$  and  $p_s$  do not matter for the spectrum shape produced by SSSS spots. We have plotted in Figure 5 the  $C^{l\star}$  spectrum ( $\bar{p}_s = p_s$ ,  $\bar{a} = a$ , no division by  $\pi p_s^2$  in (41)) for SSSS spots with  $p_s = 0.2$  (for definiteness), with cosmic variance error bars computed from (39). A flat spectrum without any significant low  $l$  cut-off is obtained, in agreement with [2, 9]. This is a general feature for any profile whenever  $\bar{p}_s$  is sufficiently large. The only novelty is the large non-Gaussian correction to the cosmic variance in this scenario, due to the low value of  $n$  (recent reruns of [2] have shown an abnormally large cosmic variance).

### 3.4.2 Gaussian spots

In [8], on the other hand, it was found that both realistic (non-symmetric) unwindings and concentrations of gradient energy produce CMBR spots. Together, these two types of effect bring the spot number density up to  $n \approx 1$ . The spots produced by the two effects appear to be indistinguishable. Their profile is clearly non-SSSS, and is better approximated by a Gaussian profile with a small  $\bar{p}_s$ , around 0.1. A clear evaluation of  $\bar{p}_s$  has not been provided by the simulations. These simulations are essentially flat space-time simulations ([8]) in which the horizon size is ambiguously defined. Hence we leave  $\bar{p}_s$  as a free parameter. Low  $\bar{p}_s$  produce slightly tilted spectra even for intermediate  $l$  (cf. Fig. 4). A natural question is how the tilt depends on  $\bar{p}_s$ . We fitted the  $C^{l\star}$  spectra for

Missing author supplied figures Missing author supplied figures  
Missing author supplied figures Missing author supplied figures

Figure 7:  $C^{l\star}$  spectrum (middle line) with its Gaussian (lines) and full (bars) cosmic variance error bars for Gaussian profile spots with  $\bar{p}_s = 0.25, 0.2, 0.1,$  and  $0.05$ , confronted with fitting Gaussian tilted spectra with the same normalization (points).

Gaussian profiles to the inflationary type of spectra

$$C^l \propto \frac{\Gamma\left(l + \frac{n^i - 1}{2}\right)\Gamma\left(\frac{9 - n^i}{2}\right)}{\Gamma\left(l + \frac{5 - n^i}{2}\right)\Gamma\left(\frac{3 + n^i}{2}\right)} \quad (42)$$

where  $n^i$  is the spectral index. The fit was performed for  $l \in (25, 30)$ , and the resulting  $n^i = n^i(\bar{p}_s)$  function is plotted in Fig. 6. For  $\bar{p}_s > 0.15$  we find  $n^i \approx 1$ , but for  $\bar{p}_s = 0.05$  and  $\bar{p}_s = 0.1$  we have respectively  $n^i = 1.3$  and  $n^i = 1.2$ , for instance. Hence the importance of an accurate measurement for  $\bar{p}_s$  as it will provide the intermediate scale spectral index for textures. Still, this is not the end of the story. In Fig. 7 we plotted the  $C^{l\star}$  spectrum for four values of  $\bar{p}_s$  with  $1\text{-}\sigma$  cosmic variance error bars. Superposed on them are the fitting inflationary type of spectra, with their Gaussian cosmic variance error bars. If  $p_s$  is not too small, a  $1\text{-}\sigma$  differentiation between the two theories arises for  $l = 2$  and  $3$  although the cosmic confusion at intermediate  $l$  is almost 1. This is somewhat surprising, as the cosmic variance in the low  $C^l$  is very high (and even higher in texture scenarios). In spite of this, the extra suppression of low  $l$  in texture scenarios is strong enough to survive cosmic confusion. It is tempting to connect this effect with the abnormally low  $C_l$  for  $l = 2, 3$  observed by COBE. However, the experimental error bars make it unwise to draw any conclusion. This effect also shows how a concept like the spectral index  $n^i$ , coined for inflation, becomes inadequate as a texture spectra qualifier. Texture spectra have a non-uniform tilt. If  $p_s$  is very small the extra suppression, although meaningful if the cosmic variance were Gaussian (high  $n$ ), is completely drowned by the non-Gaussian excess of cosmic variance. Although somewhat disappointing, this result also signals strong non-Gaussianity for low- $l$ . At the same time as it renders the  $C^l$  spectrum useless, it suggests that a particularly strong signal ought to exist in quantities measuring non-Gaussianity.

### 3.5 An heuristic interpretation and an approximate formula

The expansion into spherical harmonics acts as a scale filter. Each harmonic selects spots with an angular scale  $\Omega^s$  smaller than  $\Omega^{l(sat)} = \frac{4\pi}{l(l+1)}$ . Whatever the spot profile, if  $\Omega^s \ll \Omega^{l(sat)}$  then  $W^{ls} \approx \Omega^s$ , but if  $\Omega^s \gg \Omega^{l(sat)}$  then  $W^{ls} \ll \Omega^s$ . In the latter case, depending on the profile,  $W^{ls}$  may either reach a plateau ( $\approx \Omega^{l(sat)}$ ) or simply decrease monotonically with  $\Omega^s$ . We can understand the shape of  $C^l(y)$  by taking this into account. For  $y : \Omega^s < \Omega^{l(sat)}$ , each texture contributes to  $C^l$  like  $\Omega^{s^2}$ , but when we add them up in the  $a_m^l$  they may interfere either constructively or destructively. As a result, only a r.m.s. fluctuation proportional to  $\sqrt{N}$  contributes to  $\sqrt{C^l}$ . The overall contribution from a given  $y$  is therefore proportional to  $N\Omega^{s^2}$ , which decreases as we go up in  $y$ . As  $y$  increases we do have more textures in the sky, but their apparent size is also much smaller, and since  $N\Omega \approx const$ , the balance makes  $C^l(y)$  decrease. For  $y : \Omega^s > \Omega^{l(sat)}$ , the filter starts to act, collecting in a given  $C^l$  a contribution from each individual texture proportional to  $W^{ls^2} \ll \Omega^{s^2}$ . This may either saturate or cut-off. Whatever the case the contribution from a given  $y$  will be proportional to  $N$  or less than that. The contribution from each texture is smaller than a constant, and  $C^l$  increases as we go up in  $y$ , simply because there are more textures creating a r.m.s. fluctuation. Hence there will be a peak in  $C^l(y)$  at  $y : \Omega^s(y) \approx \Omega^{l(sat)}$ , and we may expect that most of the contribution to a given  $C^l$  will come from the scales where the filter starts to act. The contribution from these textures is of the order  $N\Omega^{l(sat)^2}$ , and recalling that  $N\Omega^s \approx const$ , we can expect a value of  $C^l$  proportional to  $\Omega^{l(sat)} \propto 1/l^2$ . This explains why we can always expect a roughly scale-invariant spectrum in the texture scenario. The only exception to this argument is the case where the  $\Omega^s > \Omega^{l(sat)}$  regime does not exist (or is irrelevant), simply because  $\Omega^{l(sat)}$  is greater than  $\langle \Omega_1 \rangle$ , the average angular size of the last texture. This is the case for low  $l$ , which do not act as a filter for any of the texture spots, because their cut-off scale is above the angular size of the last (and largest texture). Then, the largest contribution to  $C^l$  comes from the last texture, this being the case for all  $l : \Omega^{l(sat)} \gg \langle \Omega_1 \rangle$ . The last texture contribution to these  $C^l$  is, of course, independent of  $l$ , and proportional to  $\langle \Omega_1^2 \rangle$ . Hence we can expect a white noise type of spectrum ( $C^l \propto const$ ) in this  $l$  region. In practice, the transition from white noise to scale invariance happens very quickly. We never observe a white noise regime, but only a suppression for the low  $l$ .

This heuristic argument can be converted into an approximate formula by taking the toy-hat profile and carrying out explicitly the  $C^l$  integration, starting from  $y = \langle y_1 \rangle$ . Let us define  $l_1$  as

$$\Omega_1 = \Omega^s(\langle y_1 \rangle) = \frac{4\pi}{l_1(l_1 + 1)} \quad (43)$$

Missing author supplied figures

Figure 8: Approximate spectra  $l(l+1)C^l$  for various values of  $p_s$ .

(the  $l$ -scale of the last texture), and  $l_{ls}$  as

$$\Omega^s(y_{l_s}) = \frac{4\pi}{l_{ls}(l_{ls}+1)} \quad (44)$$

(the  $l$ -scale of textures living at the last-scattering surface). Then

$$C^l \propto \int_{\Omega_{l_s}}^{\Omega_1} d\Omega \frac{W^{sl2}}{\Omega^{s2}} \propto \begin{cases} \Omega_1 - \Omega_{l_s} & \text{for } l \leq l_1 \\ 3\Omega^{l(sat)} - 2\frac{\Omega^{l(sat)2}}{\Omega_1} - \Omega^{ls} & \text{for } l \geq l_1 \end{cases} \quad (45)$$

giving mathematical expression to what we have said above. This leads to the approximate spectral formula

$$C^l \propto \begin{cases} \frac{1}{l_1(l_1+1)} - \frac{1}{l_{ls}(l_{ls}+1)} & \text{for } l \leq l_1 \\ \frac{3}{l(l+1)} - \frac{2l_1(l_1+1)}{(l(l+1))^2} - \frac{1}{l_{ls}(l_{ls}+1)} & \text{for } l \geq l_1 \end{cases} \quad (46)$$

with  $l_1 \approx 0.5/\tilde{p}_s$  and  $l_{ls} \approx 30/\tilde{p}_s$  for standard recombination, with  $\tilde{p}_s = 2\bar{p}_s$ . The approximate spectra were plotted in Fig. 8 with an arbitrary vertical scale. Confronting this with Fig. 4, we see that (46) does provide a good qualitative description of the spectra.

## 4 The two-point correlation function

The two-point correlation function  $C(\theta)$  is a tool sadly closer to experiment than the  $C^l$  spectrum (however see [14] for a more hopeful point of view). We will now show that  $C(\theta)$  is a very bad discriminator between inflationary and texture scenarios.  $C(\theta)$  is defined as

$$C(\theta) = \langle \frac{\delta T}{T}(\Omega) \frac{\delta T}{T}(\Omega') \rangle_{obs} \quad (47)$$

with  $\theta = (\widehat{\Omega}, \widehat{\Omega}')$ , ( $\Omega$  and  $\Omega'$  any two fixed directions in the sky). Making use of (17) this can be written as

$$C(\theta) = \sum_l C^l \frac{2l+1}{4\pi} P_l(\cos \theta). \quad (48)$$

The theoretical  $C(\theta)$  can be estimated from the sky average of  $\frac{\delta T}{T}(\Omega) \frac{\delta T}{T}(\Omega')$  with a fixed  $\theta = (\widehat{\Omega}, \widehat{\Omega}')$ :

$$C_{obs}(\theta) = \int \frac{d\Omega d\Omega'}{8\pi^2} \frac{\delta T}{T}(\Omega) \frac{\delta T}{T}(\Omega') \delta(\cos \theta - \cos(\widehat{\Omega}, \widehat{\Omega}')) \quad (49)$$



which after some algebra leads to

$$C_{obs}(\theta) = \sum_l C_l \frac{2l+1}{4\pi} P_l(\cos \theta) \quad (50)$$

with  $C_l$  defined as in (18). An expression for  $C(\theta)$  in texture scenarios can be found by replacing (22) in (48). It is curious that a simpler expression can be derived. Inverting the Legendre transform (15) one has

$$W^s(z, y) = \sum_l \frac{2l+1}{4\pi} W^{sl}(y) P_l(z). \quad (51)$$

If we define the Legendre-squared spot profile to be

$$W^{s(2)}(z, y) = \sum_l \frac{2l+1}{4\pi} W^{sl2}(y) P_l(z) \quad (52)$$

then the correlation function is simply

$$C(\theta) = \frac{\langle a^2 \rangle}{4\pi} \int_0^{y_{ls}} dy N(y) W^{s(2)}(\cos \theta, y). \quad (53)$$

The profile  $W^{s(2)}$  is the Legendre analogue of  $W^s \star W^s$  (where  $\star$  is the convolution) in Fourier analysis. Depending on whether the profiles are defined in the  $\theta$  or in the Legendre spaces it may be easier to use (53) or to combine (48) and (22). If one wants to take into account the telescope beam filtering, one should multiply the  $C^l$  in (48) by the square of the beam Legendre transform  $\mathcal{F}^{l2}$ . In the numerics we will use an approximation to the COBE beam  $\mathcal{F}^l = e^{-\frac{1}{2}(l+\frac{1}{2})^2 \sigma^2}$  with  $\sigma = 2\pi(10^\circ/360^\circ)$ .

We have also derived an expression for the cosmic variance in  $C_{obs}(\theta)$ . In Gaussian theories ([4] with a factor of 2 correction) we have:

$$\sigma_G^2(C_{obs}(\theta)) = \sum_l \sigma_G^2(C_l) \left( \frac{2l+1}{4\pi} \right)^2 P_l^2(\cos \theta) \quad (54)$$

with  $\sigma_G^2(C_l)$  given by (36). In the texture scenarios not only does one have to replace  $\sigma_G^2(C_l)$  by  $\sigma_{TX}^2(C_l)$  (as in (39)), but also terms in  $P_l P_{l'}$  (with  $l \neq l'$ ) appear, reflecting the inter- $l$  correlations. A rather elaborate calculation, in the moulds of Sec.3.3, brings us to

$$\sigma_{TX}^2(C_{obs}(\theta)) = \sum_{l'} V_{l'} C^l C^{l'} \frac{2l+1}{4\pi} \frac{2l'+1}{4\pi} P_l(\cos \theta) P_{l'}(\cos \theta) \quad (55)$$

with

$$V_{l'} = \frac{2\delta_{l'}}{2l+1} + \left( 1 + \frac{\sigma^2(a^2)}{\langle a^2 \rangle^2} \right) \frac{\int_0^{y_{ls}} dy N(y) W^{ls2}(y) W^{l's2}(y)}{(\int_0^{y_{ls}} dy N(y) W^{ls2}(y)) (\int_0^{y_{ls}} dy N(y) W^{l's2}(y))} \quad (56)$$

Missing author supplied figures

Figure 9:  $\epsilon(\theta)$  for Gaussian spots with  $(n = 1, p_s = 0.25)$ .

Missing author supplied figures

Figure 10:  $\sigma_{TX}^2$  (top line), and its Gaussian (bottom line), diagonal (top points), and off-diagonal (bottom points) in  $V_{ll'}$ , contributions.

where, again, we have neglected terms in  $1/N_t$ . The intensity of the non-Gaussian correction to the cosmic variance can be measured by means of the quantity

$$\epsilon(\theta) = \frac{\sigma_{TX}^2(C_{obs}(\theta)) - \sigma_G^2(C_{obs}(\theta))}{\sigma_G^2(C_{obs}(\theta))} \quad (57)$$

which depends on  $n$ ,  $\bar{p}_s$ , and the profile. The dependence on  $n$  is trivial, so we define  $\tilde{\epsilon}(p_s, \theta) = \epsilon(n, p_s, \theta).n$ . The numerator in (57) can be rewritten as  $\langle (W^{s(2)})^2 \rangle$ , showing that the variance in  $C_{obs}(\theta)$  is always larger in texture scenarios than in similar Gaussian theories. As before, we adopt the attitude that while this does reduce the predictability of the theory on  $C(\theta)$ , it also signals non-Gaussian behaviour and the need of a non-Gaussian data-analysis approach to fully make out the predictions of the theory. In particular, on angular scales where  $\epsilon \gg 1$ , we know that it is worth studying the collapsed (to two points)  $n$ -point correlation function. In Fig. 9 we divided  $\theta \in (0, \pi)$  into 100 points and plotted  $\epsilon(\theta)$  for Gaussian spots with  $(n = 1, p_s = 0.25)$ . The fact that the low  $l$  multipoles contribute to  $C(\theta)$  for all  $\theta$  distributes non-Gaussianity nearly uniformly over  $\theta$ . In Fig. 10 we analyse the various contributions to  $\sigma_{TX}^2$ , separating its Gaussian, diagonal and off-diagonal components in  $V_{ll'}$ . We note that the inter- $l$  correlations responsible for the off-diagonal elements of  $V_{ll'}$  can act so as to reduce the cosmic variance, an important fact which we shall make use of in [10]. Naturally, the subtle differences in the  $C^l$ -spectra pointed out at the end of Sec.3.4 are completely drowned in  $C(\theta)$ . As an example we have plotted in Fig. 11  $C(\theta)$  for the above texture theory, and for its fitting tilted spectrum inflationary theory. As  $C(\theta)$  spreads the low  $l$  over all  $\theta$ , the two theories come out completely confused. Note however that the normalization in the  $C^l$  and in  $C(\theta)$  can be substantially different (in Fig. 11 we used a different normalization procedure than in Fig. 7).

Figure 11:  $C(\theta)$  for Gaussian spots with ( $n = 1, p_s = 0.25$ ) with its full cosmic variance error bars, confronted with its fitting  $n = 1.001$  theory (top line at  $C(\pi)$ ).

## 5 The last texture and non-Gaussianity at low $l$

In the derivation of (22) we made use of statistics for unordered textures. However, a similar expression could have been obtained using ordered textures. In this case one should be wary for the  $W_n^{sl}$  are not independent variables. Nevertheless formula (21) remains valid if one uses the marginal distribution functions of  $y_n$  in computing  $\langle W_n^{sl2} \rangle$  for each term in (21). The marginal distribution functions  $\bar{P}_n(y_n)$  are defined as

$$\bar{P}_n(y_n) = \int dy_1 \dots dy_{n-1} dy_{n+1} \dots dy_{N_t} P_{1 \dots N_t}(y_1, \dots, y_{N_t}) \quad (58)$$

and using (10) they can be found to be

$$\bar{P}_n(y_n) = N(y_n) e^{-M(y_n)} \frac{M^{n-1}(y_n)}{(n-1)!} \quad (59)$$

where  $M(y) = \int_0^y N(x) dx$ . Then:

$$C^l = \frac{\langle a^2 \rangle}{4\pi} \sum_{n=1}^{N_t} \int_0^{y_{ls}} dy_n N(y_n) W^{ls2}(y_n) e^{-M(y_n)} \frac{M^{n-1}(y_n)}{(n-1)!} \quad (60)$$

and since  $N_t$  is very large we recover (22). The advantage of (60) is that it allows us to write

$$C^l = \sum_n C_n^l \quad (61)$$

with

$$C_n^l = \frac{\langle a^2 \rangle}{4\pi} \int_0^{y_{ls}} dy_n N(y_n) W^{ls2}(y_n) e^{-M(y_n)} \frac{M^{n-1}(y_n)}{(n-1)!} \quad (62)$$

reporting the contribution of the  $n^{th}$  texture to the multipole  $C^l$ . In Figure 12 we plotted the  $C^{l*}$  spectrum for four plausible scenarios: for a Gaussian profile with  $p_s = 0.05$  and  $p_s = 0.1$  ( $n = 1$  in both cases), and for a SSSS profile with  $n = 0.25$  and  $n = 0.1$  ( $p_s = 0.2$  for both). Underneath the spectra we plotted the result of stopping the sum (61) at  $N_t$  from 1 to 10, thus obtaining the contribution of the first 10 textures to each  $C^l$ . In all the cases considered we notice that the low

Missing author supplied figures Missing author supplied figures  
 Missing author supplied figures Missing author supplied figures

Figure 12: Contribution of the last ten textures for a Gaussian profile, with  $p_s = 0.05$  and  $p_s = 0.1$  ( $n = 1$  in both cases), and for a SSSS profile with  $n = 0.25$  and  $n = 0.1$  (and  $p_s = 0.2$ ).

Missing author supplied figures Missing author supplied figures  
 Missing author supplied figures Missing author supplied figures

Figure 13: The  $\alpha^2$  and  $\alpha^3$  function for a Gaussian (top), and a SSSS profile (bottom).

$l$  multipoles are dominated by the contribution from the last texture. The  $l$  at which this stops being the case depends on the spot details (profile,  $n$ ,  $p_s$ ), but  $l = 2, 3$  always seem to be subject to this effect. Also the intensity of the last texture dominance at low  $l$  depends on the spot details, the effect being notably pronounced for Gaussian profiles with low  $p_s$ . As we go up in  $l$ , the last texture becomes less prominent, but no other single texture replaces it as a dominant feature. We may ask how many textures are responsible for, say, 95% of a given  $C^l$  for high  $l$ . Using the toy hat model and performing an approximate calculation similar to the one in Sec.3.5, we can show that this number is proportional to  $l^2$ . This implies that for high  $l$  the number of defects responsible for a given  $a_m^l$  is proportional to  $l$ .

These results have far reaching consequences. If one believes in flippan applications of the central limit theorem, then one can expect the  $a_m^l$  for high  $l < 30$  to be independent Gaussian distributed random variables, as they add up a large number of independent contributions (proportional to  $l$ ). We have now shown that this argument can certainly not be repeated for the low  $l$ . In fact, our remark in Sec.3.3 that  $\sigma_{TX}^2(C_l) > \sigma_{Gauss}^2(C_l)$ , and the numerical results plotted in Fig. 3, *prove* that the  $a_m^l$  are distinctly non-Gaussian at low  $l$ . This also implies that these  $a_m^l$  are dependent random variables [11]. We can now understand better why this is so. The non-Gaussian features in the  $a_m^l$  for low  $l$  result from the fact that they are mostly due to one single lumpy object blatantly different from Gaussian noise. We may even expect the  $a_m^l$  for low  $l$  to reproduce the morphology, size, and other features of the last defect. Devising a data-analysis method capable of uncovering these features is the purpose of [10]. We should stress that both the central limit theorem and Fig. 3 strongly suggest, but still do not prove, that the  $a_m^l$  are Gaussian for high  $l < 30$ .

The non-Gaussian toy model studied in [11] showed in which way the low  $l$

multipoles would display non-Gaussian behaviour if they were fully due to the last texture. The contribution from  $n > 1$  textures will soften this non-Gaussianity. Hence a plausible measure for the expected non-Gaussianity present in a low  $l$  multipole is  $\alpha^l = C_1^l/C^l$ , a quantity which depends on the profile,  $n$ , and  $p_s$ . We have computed numerically  $\alpha^2$  and  $\alpha^3$  for a Gaussian and a SSSS profile. The results are plotted in Fig. 13. A better connection between  $\alpha^l$  and detailed features of non-Gaussianity measure distribution functions will be given in [10].

## 6 What's new?

The focus in this paper was to derive for texture scenarios whatever one normally derives for Gaussian theories ( $C^l$ ,  $C(\theta)$ , and their cosmic variances). We met anomalous behaviour (eg. formulae (39) and (55)) which (theoretically) indicates non-Gaussianity, but we have left to the sequels [10] and [15] the task of developing a non-Gaussian data analysis method. On the whole, within the standard lore, the results obtained are surprisingly similar to inflationary scenarios. Still, we found a few novelties. We discovered that texture spectra are tilted, but not uniformly. Fitting a tilted spectrum for  $l \in (25, 30)$  (see Fig. 6) leaves a significant suppression of power at low  $l \in (2, 5)$  (see Fig. 7). We have also computed directly the cosmic variance error bars in  $C_l$  and  $C_{obs}(\theta)$ , and found them to be larger than in comparable Gaussian theories (see formulae (39) and (55) and Figs. 3 and 10). In fact, if the non-Gaussian correction is very large (which does happen for most of the parameter values suggested in the literature), cosmic variance drowns the otherwise  $1-\sigma$  suppression of power at low  $l$  mentioned above (see Fig. 7). However, one should not give way to despair. Large non-Gaussian corrections to cosmic variance only hint that we have not applied to the theory the right data analysis procedure. To give a flavour of [15] let us point out that as the  $C_l$  are dependent random variables in non-Gaussian theories ([11]), it may happen that *the  $C_l$  spectrum shape seen by any observer is never the average  $C^l$  spectrum shape*. A more intelligent method to make predictions on  $C_l$  spectra and to estimate global parameters in the  $C^l$  spectrum is in order. It appears that even a proper study of the  $C^l$  (or  $C_l$ ) spectrum for textures requires non-Gaussian data analysis.

The central result in this paper is undoubtedly the *proof* that texture low  $l$  multipoles are strongly non-Gaussian, and that the last texture is to be blamed for this (see Sec.5). We showed how the low  $C^l$  are mostly due to the last texture (slightly perturbed by the one after - see Fig. 12), and so we may expect the last texture's non-Gaussian features to be imparted on the low  $l$  multipoles. In [11] we proposed the use of  $m$ -structure and inter- $l$  measures to complement the  $C^l$ .  $m$ -structure measures act as multipole shape factors. Inter- $l$  measures correlate preferred directions in two multipoles. These two types of quantities are uniformly distributed in Gaussian theories. In topological defect scenarios we

can expect low  $l$  shape factors to reflect the morphology of the last defect. Hence their distributions should be non uniform, peaking at different values for, say, texture and cosmic strings. Inter- $l$  measures should also display the correlations between the various low  $l$  which are all due to the same last defect. It remains to be seen ([10]) how much cosmic confusion there is between these signals and their Gaussian counterparts.

On a lower key this paper was simply intended as an analytical model for texture CMBR skies with the greatest possible generality. We tried to leave as free parameters whatever simulations have failed to determine. The point is to find out what exactly must be decided in order to answer a particular question. We have concluded, for instance, that the  $C^l$  spectrum shape is insensitive to  $n$  or  $a$ , and depends very little on the spots' profile, once the identifications (33) and (35) have been made. The controlling parameter is  $\bar{p}_s$  which fixes the spectrum tilt at intermediate  $l$  (see Fig. 6). The spectrum normalization, on the other hand, depends on all the parameters of the model (see Sec.3.1), which must be evaluated before any prediction for the texture symmetry breaking energy or bias parameter can be made. Interestingly enough, we found that the low  $l$  non-Gaussianity effects depend only on  $n$ ,  $\bar{p}_s$ , and profile (Sec.5). These are not free parameters of the theory, so one ought to decide on this important issue purely by means of hard work.

The paradigm proposed here cannot easily be adapted to cosmic string scenarios. Neglecting non-circular spot modes is, in texture scenarios, only slightly inaccurate. The string counterpart to circular spots, line discontinuities cut-off at horizon distance (as in [16]), is definitely a much cruder approximation. More importantly, neglecting texture spot-spot correlations introduces only a small error (in fact it would not be difficult to incorporate small correlations in our model). On the contrary, the various segments of the string network form a Brownian random walk. Segments linked to each other are therefore very highly correlated, making an analytical treatment cumbersome. Uncorrelated string segments (as in [16]) are not very realistic. Overall, although we can boast a more realistic set of assumptions than [16], this is mostly due to the fact that textures are far simpler than strings. This also justifies why we can go further than [16]. We treated with greater rigour (no “ergodic” assumptions) a much broader set of models. We also managed to treat exactly (within the model) the problem of cosmic variance. Finally, greater sophistication in the statistical machinery opened doors to the issue of non-Gaussian data analysis in defect scenarios (developed further in [10, 15]).

## Acknowledgments

I would like to thank N.Turok and P.Ferreira for discussion in connection with this paper, and K.Baskerville for help in its preparation. This work was supported

by a fellowship at St.John's College, Cambridge.

## References

- [1] M.White, D.Scott, and J.Silk, *Am.Rv.Astron.Astrophys.* 32 (1994) 319.
- [2] U.Pen, D.Spergel, and N.Turok, *Phys.Rev.* D49 (1994) 692.
- [3] B.Allen, R.Caldwell, P.Shellard, A.Stebbins, and S.Veeraraghaven, *Cosmic strings confront COBE*, in *Birth of the Universe*, F. Occhiniero (ed), Rome 1994.
- [4] J.Bond and G.Efstathiou, *MNRAS* 226 (1987) 655.
- [5] P.Coles, *MNRAS* 234 (1988) 509.
- [6] R.Scaramella and N.Vittorio, *MNRAS* 263 (1993) L17.
- [7] T.Falk, R.Rangarajan, and M.Srednicky, *Ap.J.Lett.* 403 (1993) L1.
- [8] J.Borrill, E.Copeland, A.Liddle, A.Stebbins, and S.Veeraraghaven, *Phys.Rev.* D50 (1994) 2469.
- [9] R.Durrer, A.Howard, and Z.Zhou, *Phys.Rev.* D49 (1994) 681.
- [10] J.Magueijo, *The last texture: a large angle CMBR non-Gaussian signal*, in preparation.
- [11] J.Magueijo, *Phys.Lett.B* 342 (1995) 32.
- [12] R.Durrer, *Phys.Rev.* D42 (1990) 2533.
- [13] A.Stebbins and S.Veeraraghaven, *Phys.Rev.* D51 (1995) 1465.
- [14] D.Scott, *CMB anisotropies: an overview*, Report CfPA-95-TH-03.
- [15] J.Magueijo, *Non-Gaussian CMBR angular power spectra*, Report DAMTP-95-18.
- [16] L.Perivolaropoulos, *Phys.Lett.B* 298 (1993) 305; *Phys.Rev.D*48 (1993) 1530.

# Analytical modeling of large-angle CMBR anisotropies from textures

J.C.R. Magueijo

Mullard Radio Astronomy Observatory, Cavendish Laboratory  
Madingley Road  
Cambridge, CB3 0HE, UK

and

Department of Applied Mathematics and Theoretical Physics  
University of Cambridge  
Cambridge CB3 9EW, UK.

## Abstract

We propose an analytic method for predicting the large angle CMBR temperature fluctuations induced by model textures. The model makes use of only a small number of phenomenological parameters which ought to be measured from simple simulations. We derive semi-analytically the  $C^l$ -spectrum for  $2 \leq l \leq 30$  together with its associated non-Gaussian cosmic variance error bars. A slightly tilted spectrum with an extra suppression at low  $l$  is found, and we investigate the dependence of the tilt on the parameters of the model. We also produce a prediction for the two point correlation function. We find a high level of cosmic confusion between texture scenarios and standard inflationary theories in any of these quantities. However, we discover that a distinctive non-Gaussian signal ought to be expected at low  $l$ , reflecting the prominent effect of the last texture in these multipoles.

MRAO/1782  
DAMTP/94-101



# 1 Introduction

In the recent past, a large amount of work has been directed towards predicting the CMBR temperature anisotropies associated with inflationary scenarios (see [1] for a review), and with the various topological defect scenarios (e.g. [2, 3]). Inflationary scenarios are far better explored in this respect. The main reason for this is that it is easier in these models to plead ignorance of the detailed mechanism responsible for the density fluctuations of the Universe. Quantum fluctuations in the metric are a fuzzy subject, and hand-waving arguments for Gaussian fluctuations with a particular type of spectrum are normally considered acceptable. Once this is done, one is free to take advantage of the well developed and sophisticated industry of methods aimed at treating Gaussian fluctuations [4]. A precise prediction for the outcome of concrete experiments follows easily, making inflation popular with experimentalists. The state of affairs in topological defect scenarios is rather different. No lack of fundamental physics understanding hampers working out in rigour the defect network evolution and the fluctuations they induce on the matter and radiation of the Universe. The price to pay for our honesty is that a serious treatment of the problem is computationally overpowering. A reliable link between the defect network and the perturbations it induces is undoubtedly still missing. To top off the trouble, it turns out that the fluctuations induced by defects are often non-Gaussian. Setting up a data-analysis framework geared towards non-Gaussian fluctuations is virgin ground (but see [4, 5, 6, 7] for Gaussianity tests). Overall, even though defect scenarios have so far been poor in solid predictions, they have a potentially polemic value not to be discarded. Non-Gaussian data analysis does not exist partly because non-Gaussian theories are too vast a class to be treated in one go. Defect scenarios provide a motivated and topical example with which one can rehearse non-Gaussian data analysis techniques and experimental strategies.

The main technical complication in predicting CMBR fluctuations in defect scenarios arises from the fact that  $\frac{\delta T}{T}$  maps photograph the whole sky (that is, our past light cone clipped by the last scattering surface) and not just its intersection with the last scattering surface. Hence the defect network, surrounding matter, and CMBR photons have to be evolved through a large number of expansion times. The problem is usually tackled by means of full-blown simulations [2, 3]. These require access to supercomputers, and even so face severe limitations. Important issues like cosmic variance in defect scenarios have hardly been addressed. A possible computational short cut can be found if one is to assume scaling. The defects network is expected to scale, by which one means that it looks statistically the same at any time, once the network length scale is equated to the horizon distance. This suggests dividing the sky cone into cells corresponding to expansion times and horizon volumes. Scaling makes it plausible that the CMBR pattern in each of these cells is statistically the same, once some angular scaling procedure is applied to it. This being the case, all that is required from

the simulations is good statistics for the CMBR spots induced by defects inside horizon size boxes during one expansion time. Such simulations are considerably easier to perform. A prototype of this type of study is [8]. In the case of textures, the short-cut which we have described has been adopted by [9] where a “scaling-spot-throwing” process was implemented on a computer. The spots were all derived from model SSSS (self-similar and spherically symmetric) collapses. In this paper we advocate the use of analytical techniques for scaling-spot-throwing. An analytical approach allows the derivation of exact formulae for the  $C^l$ ,  $C(\theta)$ , and their cosmic variance, from which interesting general properties can be derived. These properties are naturally less evident in computer simulations, unless one explicitly sets out to find them. Furthermore, an analytical approach allows the treatment of a more general case than [9]. The method proposed here applies to quasi-circular spots with any profile. The scaling size ( $p_s$ ), number density ( $n$ ), and brightness factor ( $a$ ) of the spots are also left as free parameters. We should admit that only the brightness factor is a truly free parameter in the texture model. All others should be considered as phenomenological in origin, eventually to be fixed by simulations. As they still constitute a controversial matter, we choose to consider a broader class of model spots. We can then sort out which spot properties it is really important to measure from the simulations.

The plan of this paper is as follows. In Sec.2 we start by deriving the statistical properties of scaling texture model collapses as they appear in the sky cone, and from these a formal solution for the joint distribution function of the CMBR  $a_m^l$  is given. Using this solution, in Secs.3.1 and 3.3 we derive exact formulae for the  $C^l$  and  $\sigma(C_l)$  in texture models. We prove the general result that the cosmic variance in the  $C_l$  is larger in texture scenarios than in Gaussian theories. The excess variance is negligible for high  $l$ , but significant at low  $l$ . In Secs.3.2 and 3.4 we compute numerically the  $C^l$  spectra (with cosmic variance error bars) for a large class of spot types. We find that the spots’ profile, intensity, and number density affect only the spectrum normalization. The spectrum shape is largely controlled by the spots’ scaling size  $p_s$  alone. In general, the spectra are slightly tilted (and we numerically compute the dependence of the tilt on  $p_s$ ), but with an extra suppression of power at low  $l$ . In Sec.4 we derive expressions for the two-point correlation function  $C(\theta)$  and its cosmic variance. Although closer to experiment,  $C(\theta)$  appears to be a very bad discriminator between texture and inflationary scenarios. The most original result proved in this paper is presented in Sec.5, where we ask how many textures are responsible for a given  $a_m^l$ . For high  $l$ , this number goes like  $l$ , suggesting Gaussian behaviour. For low  $l$  we find that the  $a_m^l$  are mostly due to the effects of a single texture: the last (that is, the closest) texture. This ought to impart a peculiar non-Gaussian signal to the low  $a_m^l$ , a fact which we prove explicitly. The purpose of the sequel to this paper [10] is to devise a low- $l$  data-analysis technique (in the moulds of [11]) capable of fully characterising this effect.

## 2 Analytical spot-throwing

In topological defect scenarios the CMBR fluctuations at large angles are due only to the ISW (integrated Sachs-Wolfe) effect caused by the defect network ([2]). For a standard recombination scenario the validity range for this approximation is  $2 \leq l \leq 30$ . If early reionization occurs, the upper limit for this range becomes the value of  $l$  corresponding to the angular scale of the horizon at “last scattering” (defined in some conservative way). As it is not clear which is the most sensible scenario we take as a working hypothesis the choice which maximizes the applicability of our model: standard recombination. Now if we assume that the statistical scaling of the texture fields extends to their associated time-dependent metric perturbations, then we may expect the ISW spots themselves to scale. This allows the direct modelling of the statistics for texture induced spots as they appear in the sky. From these, we can then write an expression for the  $a_m^l$  joint distribution function for  $2 \leq l \leq 30$ . For simplicity, we will assume that the texture spots are independent (not required by the formalism, but a good approximation). Then each texture angular position in the sky is uniformly distributed. Furthermore its time position in the sky cone can be associated with a modified Poisson process in time, in which the probability of an event is allowed to vary. Let  $n$  be the average number of texture spot producing configurations per horizon volume. Then their average volume density is

$$\rho = \frac{2n}{9\pi t^3} \quad (1)$$

and using the relation between the proper area  $dS$ , the time of emission  $t$ , and the apparent solid angle  $d\Omega$ :

$$dS = d\Omega \left( 3t \left( \left( \frac{t_0}{t} \right)^{1/3} - 1 \right) \right)^2 \quad (2)$$

we find that the angular density of spots in the sky per unit of emission time is

$$\delta(t) = \frac{2n}{\pi t} \left( \left( \frac{t_0}{t} \right)^{1/3} - 1 \right)^2. \quad (3)$$

It is convenient to introduce the variable  $y = \log_2(t_0/t)$ , the expansion time number as we go backwards in time. Each  $\Delta y = 1$  represents one expansion time, starting from  $y_0 = 0$  (here and now) and going as far as  $y_{ls} = \log_2(t_0/t_{ls})$ , when we hit the last scattering surface. In the standard recombination scenario  $y_{ls} \approx 15$ . In terms of  $y$  the spot density in the sky is

$$N(y) = 2n \log(2) \left( 2^{y/3} - 1 \right)^2. \quad (4)$$

Let us now introduce a Poisson-type process in  $y$ , with a variable probability density  $N(y)$ . If  $p_n(y)$  is the probability of having exactly  $n$  textures at  $y' < y$ , then

$$\frac{dp_n}{dy} = N(y)(p_{n-1} - p_n) \quad , \quad p_{-1} = 0 . \quad (5)$$

This hierarchy of equations fully specifies the statistics of the textures' time-position in the sky. From the  $p_n(y)$  one can also derive the probability density of the  $n^{\text{th}}$  texture position  $y_n$  by means of

$$P_n(y_n) = p_{n-1}(y_n)N(y_n) . \quad (6)$$

However one should be wary of the  $y_n$  variables, as they are not independent. Not only are their ranges constrained by  $y_1 < y_2 < \dots < y_n$  but also their statistical dependence is patent in the conditional distribution functions. From (5) and (6) one has that

$$P_1(y_1) = N(y_1)e^{-\int_0^{y_1} dy N(y)} \quad (7)$$

but then

$$P_2(y_2|y_1) = N(y_2)e^{-\int_{y_1}^{y_2} dy N(y)} \quad (8)$$

which is dependent on  $y_1$ . From these expressions we can derive the joint distribution function

$$P_{12}(y_1, y_2) = N(y_1)N(y_2)e^{-\int_0^{y_2} dy N(y)} \quad (9)$$

which misleadingly factorizes. More generally one has

$$P_{1\dots n}(y_1, y_2, \dots, y_n) = N(y_1)N(y_2)\dots N(y_n)e^{-\int_0^{y_n} dy N(y)} . \quad (10)$$

The statistics contained in  $P_n$  or  $p_n$  refer to a sequence of textures ordered in  $y$ . Ordering will be crucial in Section 5 when we uncover the last texture. However for some other purposes (like the derivations in Section 3) we may simply consider unordered textures. Then we have a total of  $N_t = \int_0^{y_t} dy N(y) \gg 1$  textures in the sky. Their positions  $y_n$  are independent random variables with a distribution

$$P_n(y_n) = \frac{N(y_n)}{N_t} \quad (11)$$

for all  $n$ , which is considerably simpler.

We now model the texture spot patterns. These ought to follow some sort of statistical scaling law, where the scale angle is

$$\theta^s(y) = \arcsin \left( \min \left( 1, \frac{p_s}{2y^{1/3} - 1} \right) \right) \quad (12)$$

for a pattern laid at time  $y$ . Here  $p_s$  is the scaled impact parameter ( $p_s = p/(3t)$ ) giving  $\sigma_s = \pi p_s^2$ , the scaled cross section for photon anisotropies. Causality requires that  $p_s < 1/2$ . It may happen that  $p_s$  is a random variable itself, but

we shall ignore this complication. For small, nearly circular spots with profile  $W^s(\theta, y)$ , scaling implies that

$$W^s(\theta, y) = \overline{W}(x) \quad (13)$$

with  $x = \theta/\theta^s$ . This is a sensible scaling law even for  $y < 1$ , although for  $y < 1$  the exact scaling law should be more complicated, as the photons propagating through the scaling metric no longer move along parallel trajectories. In particular, if  $y < y_0 = 3 \log(1 + p_s)$ , we live inside a texture and are enclosed by its pattern. Unless  $(2np_s)^3 \approx 1$  textures like these are very rare, and the approximation (13) should produce good enough final results.

We seek to write the  $a_m^l$  coefficients for skies filled with nearly circular spots described by the above statistics. For each of these spots let us first point the  $z$ -axis at their centre, and perform the spherical harmonic decomposition in that frame. We obtain an expression of the form

$$\tilde{a}_m^l(n) = a_n W^{sl}(y_n) \cdot \sqrt{\frac{2l+1}{4\pi}} \cdot \delta_{m0} + \epsilon_m^l \quad (14)$$

where  $W^{sl}$  is the Legendre transform of the scaled profile:

$$W^{sl} = 2\pi \int_{-1}^1 dz P^l(z) W^s(z, y_n) \quad (15)$$

and  $\epsilon_m^l$  is a perturbation induced by the eccentricity. This perturbation is negligible, even if the spots are not very nearly circular, but  $l \ll [1/\theta^s(y_n)]$ . The extra factor  $a_n$  in (15) accounts for the texture brightness, and is a random variable with a  $y_n$ -independent distribution function. Performing a rotation to a general frame, where the  $n^{\text{th}}$  texture has coordinates  $\Omega_n$ , and summing over all textures one finally obtains:

$$a_m^l = \sum_n a_n W^{sl}(y_n) Y_m^{l*}(\Omega_n) . \quad (16)$$

The variables  $a_n$  are independent but equally distributed. Their distribution has to be determined from the simulations. The  $\Omega_n$  are uniformly distributed, and from them one can determine the  $Y_m^l(\Omega_n)$  distributions (but with care, as the  $Y_m^l$  are not independent). Finally from (10), (12), and (15) one can determine the  $W_n^{sl}$  distributions. The  $W_n^{sl}$  makes the various terms in (16) dependent variables, rendering an analytic approach for the  $a_m^l$  distributions through (16) unfeasible. In any case finding the marginal distributions of the  $a_m^l$  would not be the end of the story, since the  $a_m^l$  are necessarily dependent random variables (see [11]). Hence we still would have to find the joint distribution  $F(a_{m_1}^1, a_{m_2}^2, \dots)$  for a complete solution to the problem of cosmic variance in texture scenarios. Expression (16) constitutes a formal solution to this problem which, despite all the obstacles to an analytical solution, is particularly suited to Monte Carlo simulations. It

separates the individual effect of each texture on each of the  $a_m^l$ . It also factorizes each texture contribution into three factors. The  $Y_m^{l*}$  are purely geometrical factors which should be present in any SSS (statistically spherically symmetric) theory (see [11] for a definition). The  $W_n^{sl}$  are a reflection of the structure of the sky (foliation into expansion times and horizon volumes) and should be present whenever there is scaling. Finally, the  $a_n$ 's factor out all that is peculiar to the texture model under consideration, and will have to be measured from detailed texture simulations.

### 3 The angular power spectrum

#### 3.1 An expression for the $C^l$

Throughout this paper we will use the notation  $C_l$  for the angular power spectrum of realizations, and  $C^l$  for its ensemble average. Whereas  $C_l$  is a random variable,  $C^l$  is a number. In any SSS theory one has

$$\langle a_m^l a_{m'}^{l*} \rangle_{obs} = C^l \delta_{ll'}^l \delta_{mm'}^m . \quad (17)$$

The  $C^l$  can be estimated from the observable

$$C_l = \frac{1}{2l+1} \sum_{m=-l}^l |a_m^l|^2 \quad (18)$$

since  $\langle C_l \rangle_{obs} = C^l$  in any SSS theory. Cosmic variance introduces error bars of size  $\sigma(C_l)$  into this estimate. We start by deriving an exact expression for the  $C^l$ . From (16) and (18) we have that

$$C^l = \langle C_l \rangle = \frac{1}{2l+1} \sum_m \sum_{nn'} \langle a_n a_{n'} \rangle \langle W_n^l W_{n'}^l \rangle \langle Y_m^{l*}(\Omega_n) Y_m^l(\Omega_{n'}) \rangle \quad (19)$$

but since

$$\langle Y_m^{l*}(\Omega_n) Y_m^l(\Omega_{n'}) \rangle_{obs} = \frac{\delta_{nn'}}{4\pi} \quad (20)$$

we have simply

$$C^l = \frac{\langle a^2 \rangle}{4\pi} \sum_n \langle W_n^{l2} \rangle . \quad (21)$$

Computing the averages using the unordered statistical description (11) we can write

$$C^l = \frac{\langle a^2 \rangle}{4\pi} \int_0^{y_{ls}} dy N(y) W^{ls2}(y) . \quad (22)$$

If  $p_s$  is a random variable with distribution  $f(p_s)$ , then expression (22) still holds but now with  $W^{sl2}$  replaced by  $\int dp_s f(p_s) W^{sl2}(y, p_s)$ . Expression (22) lends itself to be written as

$$C^l = \int_0^{y_{ls}} dy C^l(y) \quad (23)$$

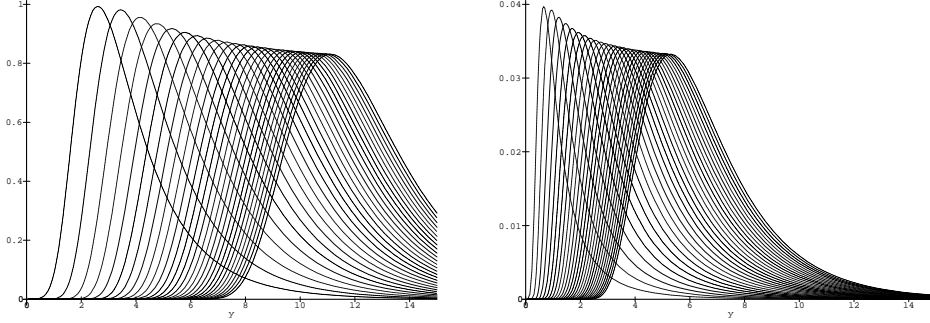


Figure 1: The density  $C^l(y)$  multiplied by  $l(l+1)$  for  $l$  from 2 to 30 for  $(n = 1, p_s = 0.4)$  and  $(n = 1, p_s = 0.08)$  textures with Gaussian profile spots.

thus defining a density

$$C^l(y) = \frac{\langle a^2 \rangle}{4\pi} N(y) \overline{W^{ls2}}(y) \quad (24)$$

measuring the contribution of textures living at time  $y$  to a given  $C^l$ . In Fig. 1 we have plotted  $l(l+1)C^l(y)$  for  $(n = 1, p_s = 0.4)$  and  $(n = 1, p_s = 0.08)$  textures with Gaussian profile spots, for  $l$  from 2 to 30. These plots are to be confronted with the common belief that a given  $C^l$  is mostly due to textures living at a time when the apparent size of the horizon equals the multipole angular scale. We find instead that  $C^l(y)$  peaks for  $y: \Omega^s(y) \approx \frac{4\pi}{l(l+1)}$ , that is, when the textures' apparent size fits the multipole angular scale. Furthermore the peaks comprise several generations and an accurate prediction for the  $C^l$  spectrum can never neglect any of the integrand in (23). Changing  $n$  only affects the normalization of  $C^l(y)$ . Reducing  $p_s$  not only decreases the normalization but also shifts the peaks to the left necessarily affecting the shape of the integrated  $C^l$ . In general as  $l$  increases the peak's heights (multiplied by  $l(l+1)$ ) are slightly reduced, but their width increases. The delicate balance of these two effects will determine whether the  $C^l$  spectrum is flat or not.

### 3.2 Profiles and reduced $a$ and $p_s$

It is not clear what profile  $\overline{W}$  real texture spots have. Simulations [2, 8] suggest that the well-known SSSS profile may be oversimplified. We find that the exact profile form has little impact on the  $C^l$ -spectra. For intermediate  $l$ , profiles do not matter at all, and for low  $l$  they induce differences easily confused by cosmic variance. The issue of matching free parameters for different profiles is, however, non-trivial. We have considered the following profiles:

1.-**Hat profile.** Defined by

$$\overline{W}^s(x) = H(1 - x) \quad (25)$$

where  $H$  is the Heaviside function. Its Legendre transform is

$$W^{sl} = 2\pi \int_{\cos \theta^s}^1 dz P^l(z) = \frac{2\pi}{2l+1} (P_{l+1}(\cos \theta^s) - P_{l-1}(\cos \theta^s)), \quad (26)$$

the  $l$ -weighted scaled solid angle.

2.-**Toy hat profile.** We can skip the complications induced by the Legendre polynomials approximating the hat profile by

$$W^{sl2} = \begin{cases} \Omega^{s2} & \text{for } \Omega^s < \Omega^{l(sat)} = \frac{4\pi}{l(l+1)} \\ \Omega^{l(sat)2} & \text{for } \Omega^s > \Omega^{l(sat)} \end{cases} \quad (27)$$

with

$$\Omega^s = 2\pi(1 - \cos \theta^s). \quad (28)$$

the scaled solid angle.

3.-**Gaussian profile.** A large angle generalization of the well-known small angle Gaussian window:

$$W^{ls} = \Omega^s e^{-\frac{(l+\frac{1}{2})^2 \theta^{s2}}{2}}. \quad (29)$$

4.-**SSSS profile.** A profile of the form (e.g. [12])

$$W^s(\theta, y) \propto \frac{\theta^s}{\sqrt{2\theta^{s2} + \theta^2}} \quad (30)$$

with some sort of cut off at

$$\theta^h(y) = \arcsin \left( \min \left( 1, \frac{1/2}{2y/3 - 1} \right) \right) \quad (31)$$

the angle subtended by the horizon. We define this cut off with the Legendre transform:

$$W^{sl} = \begin{cases} 2\pi \theta^h \theta^s e^{-\sqrt{2}\theta^s/\theta^h} & \text{for } l \leq [1/\theta^h] \\ 2\pi \theta^s \frac{e^{-\sqrt{2}\theta^s l}}{l} & \text{for } l \geq [1/\theta^h]. \end{cases} \quad (32)$$

The hat profile is suggested by the belief that  $\frac{\delta T}{T}$  circular averages are all that matters for  $2 \leq l \leq 30$ . Circular averages have been extensively studied (eg. [13]) and some useful properties have been found for them. The toy hat profile, due to its simplicity, is ideal for an heuristic explanation of the results obtained (Sec.3.5). The Gaussian profile is particularly amenable to analytical work, thus providing a good check on the numerics. Furthermore it is probably a good approximation to the peaks found in [8]. Finally, there is no harm in



considering the SSSS profile, for it might have something to do with reality after all.

With the  $\overline{W}$  defined as they are, the functions  $C^l(y)$  peak for different values of  $y$ . To facilitate comparison we should therefore define a reduced  $p_s$ :

$$\overline{p}_s = \frac{p^{hat}}{1.8} = \frac{p^{toy}}{2} = p^{gauss} \quad (33)$$

which ensures that, for high  $l$ ,  $C^l(y)$  peaks at the same  $y_{max}$  for the same  $\overline{p}_s$  for all profiles. For the SSSS profile  $C^l(y)$  peaks always for  $y : \theta^h(y) \approx \frac{1}{l}$ . This is understandable as the integrated anisotropy increases logarithmically as we go away from the core. As a result, the effective cross-section for SSSS textures is the horizon area, for all  $p_s$ . For this reason we will always treat the SSSS profile separately, as it does not really have a parameter  $p_s$ .

It also happens that the value of  $C^l(y_{max})$  depends on the profile, taking the form

$$C^l(y_{max}) = \frac{\langle a^2 \rangle .2n \log(2) .\pi p_s^2}{l(l+1)} .\alpha \quad (34)$$

with  $\alpha^{hat} \approx 0.58$ ,  $\alpha^{toy} = 1$ ,  $\alpha^{gauss} = 1/(4e)$ . By defining a reduced  $a$  as

$$\overline{a} = a \sqrt{\alpha} \frac{p_s}{\overline{p}_s} = 1.05 a^{hat} = 2a^{toy} = \frac{a^{gauss}}{2\sqrt{e}} \quad (35)$$

we can ensure that  $C^l(y_{max})$  for high  $l$  is the same for all the profiles with the same  $\langle \overline{a}^2 \rangle$  and  $\overline{p}_s$ .

In Fig. 2 we have plotted  $C^{20}(y)$  in units of  $\langle \overline{a}^2 \rangle n$ , with  $\overline{p}_s = 0.2$ , for the first three profiles proposed. We notice that for  $y > y_{max}$  all the  $C^l(y)$  have the same form, as for all profiles  $W^{ls} \propto \Omega^s$  (even though the proportionality constants may be different). Consequently, in this region  $C^l(y) \propto \Omega^s(y) \propto 1/N(y)$  regardless of the profile. For  $y \ll y_{max}$  we have  $W^{ls} \ll \Omega^s$  and so  $C^l(y)$  is proportional to  $N(y)$  or smaller than that. The exact form of  $C^l(y)$  in this region is profile dependent, as it involves details of how  $W^{ls}(\Omega^s)$  starts to cut off at a particular scale. While this portion of the integrand is not the main contribution to the total  $C^l$  it is clear that the detailed form of the spectrum is going to be profile dependent. It remains to be seen if these differences have any meaning once cosmic variance error bars are taken into account.

It is also in the  $y \ll y_{max}$  region that  $C^l(y)$  may be affected by the existence of non-spherical spot modes ( $\epsilon_m^l$  in (14)). These are the only source of inaccuracies in the model proposed, and so whatever mistakes we make will be in this region. Like profile differences, spots' ellipticity can only affect the final  $C^l$  in the fine detail. Most probably, ellipticity affects  $C^l$  even less than the profile, as the spots seen in the simulations appear to be very circular.

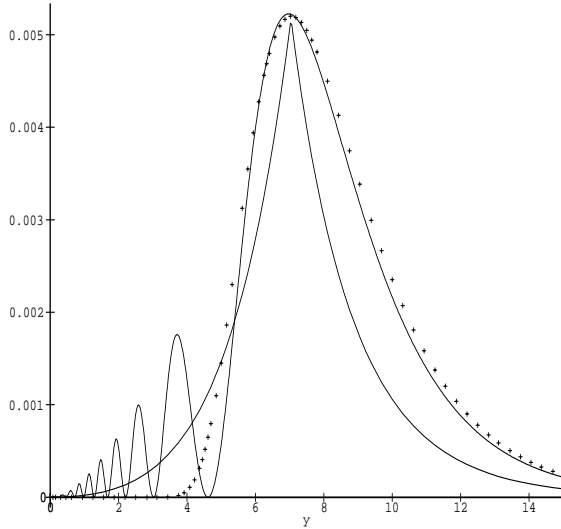


Figure 2:  $C^{20}(y)$  for the hat profile (oscillating line), the toy hat profile (non-oscillating line), and Gaussian profile (with points). For all the curves  $\bar{p}_s = 0.2$  and  $\langle \bar{a}^2 \rangle$  is the same.

### 3.3 An expression for $\sigma^2(C_l)$

We now turn to the issue of cosmic variance in the  $C_l$ . This turns out to depend on the nature of the theory. It is known that in Gaussian theories the  $C_l$  are  $\chi^2_{2l+1}$ -distributed with a variance

$$\sigma_G^2(C_l) = C^{l2} \frac{2}{2l+1} . \quad (36)$$

In some of the literature these are also the cosmic variance error bars attributed to non-Gaussian theories. We will use our model to compute directly  $\sigma_{TX}^2(C_l)$ . From (16) we have that

$$\begin{aligned} \langle C_l^2 \rangle_{obs} &= \frac{1}{(2l+1)^2} \sum_{mm'} \sum_{(n_1 n_2 n_3 n_4)} \langle a_{n_1} a_{n_2} a_{n_3} a_{n_4} \rangle \langle W_{n_1}^l W_{n_2}^l W_{n_3}^l W_{n_4}^l \rangle \\ &\quad \langle Y_m^{l*}(\Omega_{n_1}) Y_m^l(\Omega_{n_2}) Y_{m'}^{l*}(\Omega_{n_3}) Y_{m'}^l(\Omega_{n_4}) \rangle . \end{aligned} \quad (37)$$

The last factor can only be non-zero in one of the following cases:

- if  $n_1 = n_2$  and  $n_3 = n_4$  but  $n_1 \neq n_3$ , giving rise to  $(2l+1)^2$  terms,
- if  $n_1 = n_3$  and  $n_2 = n_4$  (but  $n_1 \neq n_2$ ) or  $n_1 = n_4$  and  $n_2 = n_3$  (but  $n_1 \neq n_2$ ), giving rise to a total of  $2(2l+1)$  terms,
- if  $n_1 = n_2 = n_3 = n_4$ , giving rise to a single term.

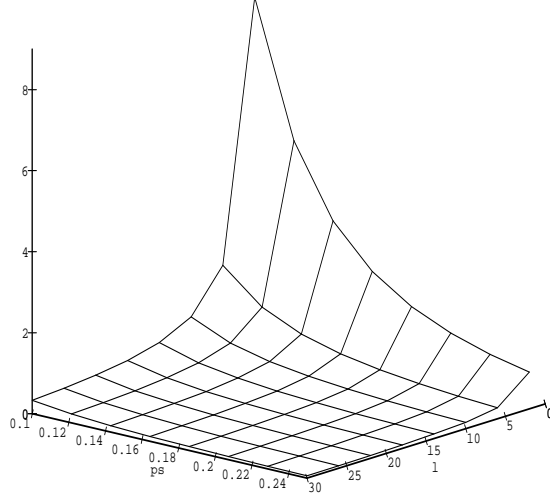


Figure 3: The relative non-Gaussian excess variance  $\tilde{\epsilon}^l(p_s)$  for Gaussian profile spots.

Putting all these terms together one has

$$\langle C_l^2 \rangle_{obs} = \frac{\langle a^2 \rangle^2}{(4\pi)^2} \sum_{n \neq n'} \langle W_n^{l2} W_{n'}^{l2} \rangle \left( 1 + \frac{2}{2l+1} \right) + \frac{\langle a^4 \rangle}{(4\pi)^2} \sum_n \langle W_n^{l4} \rangle . \quad (38)$$

Subtracting off  $C^{l2}$  written as (21), using (11), and neglecting terms in  $1/N_t$ , one finds after some algebra

$$\sigma_{TX}^2(C_l) = C^{l2} \left( \frac{2}{2l+1} + \left( 1 + \frac{\sigma^2(a^2)}{\langle a^2 \rangle^2} \right) \frac{\int_0^{y_{l_s}} dy N(y) W^{ls4}(y)}{\left( \int_0^{y_{l_s}} dy N(y) W^{ls2}(y) \right)^2} \right) . \quad (39)$$

We note that the cosmic variance in the  $C^l$  in texture scenarios is always larger than in Gaussian theories. We define  $\epsilon^l$ , the relative size of the excess variance, as

$$\epsilon^l = \frac{\sigma_{TX}^2(C_l) - \sigma_G^2(C_l)}{\sigma_G^2(C_l)} . \quad (40)$$

$\epsilon^l$  is a function of  $n$ ,  $p_s$ , and the profile. In general  $\epsilon^l(n, p_s) = \epsilon^l(1, p_s)/n$ , so we define  $\tilde{\epsilon}^l(p_s) = \epsilon^l(1, p_s)$ , the excess variance per unit of  $1/n$ . The quantity  $\epsilon^l$  can be seen as a (theoretical) indicator of how non-Gaussian a given multipole is. A texture theory with  $n \rightarrow \infty$  will be a Gaussian theory. A low  $n$  theory will be very non-Gaussian, at least for some  $l$ . In Fig. 3 we have plotted  $\tilde{\epsilon}^l(p_s)$  for spots with a Gaussian profile. Generally the excess variance is very small for high  $l < 30$ . For low  $l$  (say from 2 to 5) the correction can be considerable, the more so the smaller the  $p_s$ .

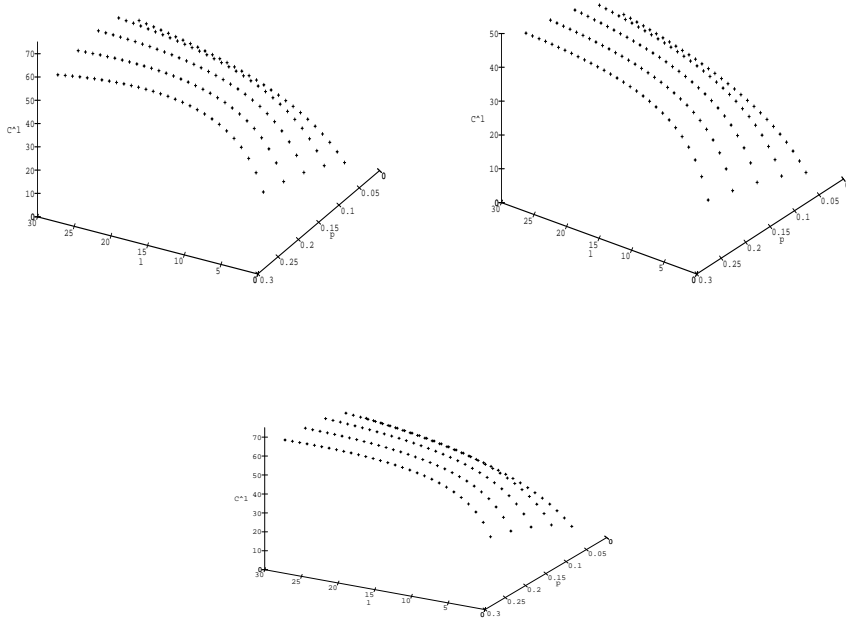


Figure 4:  $C^{l*}$  spectra for the hat, toy hat, and Gaussian profiles.

### 3.4 $C^{l*}$ -spectra for different $\bar{p}_s$ and profiles

From (24) we see that the parameters  $\langle a^2 \rangle$  and  $n$  can only affect the overall normalization of the spectrum. Also (34) suggests that the “average” spectrum normalization is proportional to  $\pi p_s^2$ , although  $p_s$  may affect the spectrum shape as well. Furthermore a roughly scale invariant ( $\propto 1/l^2$ ) spectrum can be expected. We do want more than a rough prediction, though, so we define a reduced spectrum

$$C^{l*} = \frac{4\pi l(l+1)C^l}{\langle \bar{a}^2 \rangle \cdot 2n \log(2) \cdot \pi \bar{p}_s^2} . \quad (41)$$

$C^{l*}$  describes in detail departures from scale invariance and factors out all that contributes only to the normalization of the spectrum. It depends only on the profile and  $\bar{p}_s$ . In Fig. 4 we have plotted the  $C^{l*}$  spectrum for various values of  $\bar{p}_s \leq 1/4$  (to ensure causality), for the hat, toy hat, and Gaussian profiles. The spectrum normalization still depends on the profile. Even though the peak heights in  $C^l(y)$  have been matched by our definitions of  $\bar{p}_s$  and  $\bar{a}$ , the differences in the peak’s shapes and in  $C^l(y)$  away from the peak produce different integrated

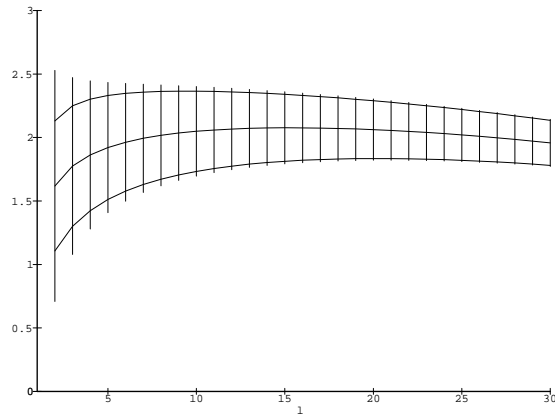


Figure 5:  $C^{l*}$  spectrum (middle line) and its Gaussian (lines) and non-Gaussian (bars) cosmic variance error bars for spots with a SSSS profile with  $n=0.25$  and  $p_s = 0.2$ .

$C^l$  for different profiles. Apart from this it is remarkable that the  $C^{l*}(\bar{p}_s)$  spectra shapes do not depend on the profile in any significant way. For intermediate scales ( $l_1 < l < 30$ , for some  $l_1$ ), the spectra are scale-invariant if  $\bar{p}_s$  is not too small. If  $\bar{p}_s$  is small, the spectrum is slightly tilted. Whatever the case, for low  $l$  ( $l < l_1$ ) the power is suppressed relative to a scale invariant (or slightly tilted) spectrum. An exact evaluation of the tilt,  $l_1$ , and low  $l$  suppression factor can only be done numerically. An approximate formula and heuristic explanation of this effect is given in Sec.3.5.

### 3.4.1 SSSS collapses

We have applied our formalism to concrete choices of  $(n, \bar{p}_s)$  and profile which have often been suggested by simulations. In [9] there is the suggestion that it is a good approximation to consider that only SSSS collapses followed by unwindings cause CMBR spots. This leads to a scenario with a low spot number density ( $n \approx 0.25$ ), and regardless of  $p_s$  (which is a random variable in this case), to an effective spot size of the order of the horizon angular size. We have pointed out before that  $n$  and  $p_s$  do not matter for the spectrum shape produced by SSSS spots. We have plotted in Figure 5 the  $C^{l*}$  spectrum ( $\bar{p}_s = p_s$ ,  $\bar{a} = a$ , no division by  $\pi p_s^2$  in (41)) for SSSS spots with  $p_s = 0.2$  (for definiteness), with cosmic variance error bars computed from (39). A flat spectrum without any significant low  $l$  cut-off is obtained, in agreement with [2, 9]. This is a general feature for any profile whenever  $\bar{p}_s$  is sufficiently large. The only novelty is the large non-Gaussian correction to the cosmic variance in this scenario, due to the low value of  $n$  (recent reruns of [2] have shown an abnormally large cosmic variance).

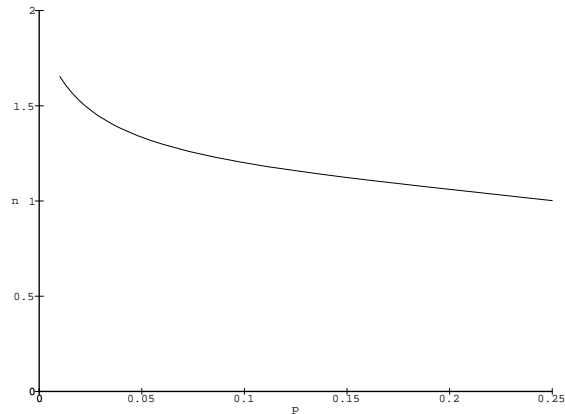


Figure 6: The spectral index  $n^i$  for high  $l$  as a function of  $\bar{p}_s$ .

### 3.4.2 Gaussian spots

In [8], on the other hand, it was found that both realistic (non-symmetric) unwindings and concentrations of gradient energy produce CMBR spots. Together, these two types of effect bring the spot number density up to  $n \approx 1$ . The spots produced by the two effects appear to be indistinguishable. Their profile is clearly non-SSSS, and is better approximated by a Gaussian profile with a small  $\bar{p}_s$ , around 0.1. A clear evaluation of  $\bar{p}_s$  has not been provided by the simulations. These simulations are essentially flat space-time simulations ([8]) in which the horizon size is ambiguously defined. Hence we leave  $\bar{p}_s$  as a free parameter. Low  $\bar{p}_s$  produce slightly tilted spectra even for intermediate  $l$  (cf. Fig. 4). A natural question is how the tilt depends on  $\bar{p}_s$ . We fitted the  $C^{l*}$  spectra for Gaussian profiles to the inflationary type of spectra

$$C^l \propto \frac{\Gamma\left(l + \frac{n^i - 1}{2}\right) \Gamma\left(\frac{9 - n^i}{2}\right)}{\Gamma\left(l + \frac{5 - n^i}{2}\right) \Gamma\left(\frac{3 + n^i}{2}\right)} \quad (42)$$

where  $n^i$  is the spectral index. The fit was performed for  $l \in (25, 30)$ , and the resulting  $n^i = n^i(\bar{p}_s)$  function is plotted in Fig. 6. For  $\bar{p}_s > 0.15$  we find  $n^i \approx 1$ , but for  $\bar{p}_s = 0.05$  and  $\bar{p}_s = 0.1$  we have respectively  $n^i = 1.3$  and  $n^i = 1.2$ , for instance. Hence the importance of an accurate measurement for  $\bar{p}_s$  as it will provide the intermediate scale spectral index for textures. Still, this is not the end of the story. In Fig. 7 we plotted the  $C^{l*}$  spectrum for four values of  $\bar{p}_s$  with  $1\text{-}\sigma$  cosmic variance error bars. Superposed on them are the fitting inflationary type of spectra, with their Gaussian cosmic variance error bars. If  $p_s$  is not too small, a  $1\text{-}\sigma$  differentiation between the two theories arises for  $l = 2$  and  $3$  although the cosmic confusion at intermediate  $l$  is almost 1. This is somewhat surprising, as the cosmic variance in the low  $C^l$  is very high (and even higher in texture scenarios). In spite of this, the extra suppression of low  $l$  in texture

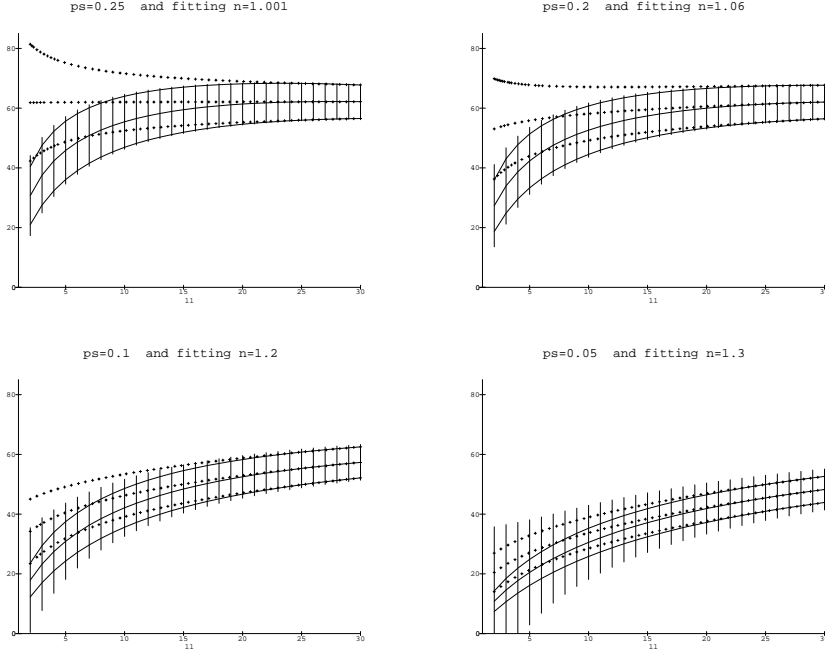


Figure 7:  $C^{l*}$  spectrum (middle line) with its Gaussian (lines) and full (bars) cosmic variance error bars for Gaussian profile spots with  $\bar{p}_s = 0.25, 0.2, 0.1,$  and  $0.05$ , confronted with fitting Gaussian tilted spectra with the same normalization (points).

scenarios is strong enough to survive cosmic confusion. It is tempting to connect this effect with the abnormally low  $C_l$  for  $l = 2, 3$  observed by COBE. However, the experimental error bars make it unwise to draw any conclusion. This effect also shows how a concept like the spectral index  $n^i$ , coined for inflation, becomes inadequate as a texture spectra qualifier. Texture spectra have a non-uniform tilt. If  $p_s$  is very small the extra suppression, although meaningful if the cosmic variance were Gaussian (high  $n$ ), is completely drowned by the non-Gaussian excess of cosmic variance. Although somewhat disappointing, this result also signals strong non-Gaussianity for low- $l$ . At the same time as it renders the  $C^l$  spectrum useless, it suggests that a particularly strong signal ought to exist in quantities measuring non-Gaussianity.

### 3.5 An heuristic interpretation and an approximate formula

The expansion into spherical harmonics acts as a scale filter. Each harmonic selects spots with an angular scale  $\Omega^s$  smaller than  $\Omega^{l(sat)} = \frac{4\pi}{l(l+1)}$ . Whatever the spot profile, if  $\Omega^s \ll \Omega^{l(sat)}$  then  $W^{ls} \approx \Omega^s$ , but if  $\Omega^s \gg \Omega^{l(sat)}$  then  $W^{ls} \ll \Omega^s$ . In the latter case, depending on the profile,  $W^{ls}$  may either reach a plateau ( $\approx \Omega^{l(sat)}$ ) or simply decrease monotonically with  $\Omega^s$ . We can understand the shape of  $C^l(y)$  by taking this into account. For  $y : \Omega^s < \Omega^{l(sat)}$ , each texture contributes to  $C^l$  like  $\Omega^{s^2}$ , but when we add them up in the  $a_m^l$  they may interfere either constructively or destructively. As a result, only a r.m.s. fluctuation proportional to  $\sqrt{N}$  contributes to  $\sqrt{C^l}$ . The overall contribution from a given  $y$  is therefore proportional to  $N\Omega^{s^2}$ , which decreases as we go up in  $y$ . As  $y$  increases we do have more textures in the sky, but their apparent size is also much smaller, and since  $N\Omega \approx const$ , the balance makes  $C^l(y)$  decrease. For  $y : \Omega^s > \Omega^{l(sat)}$ , the filter starts to act, collecting in a given  $C^l$  a contribution from each individual texture proportional to  $W^{ls^2} \ll \Omega^{s^2}$ . This may either saturate or cut-off. Whatever the case the contribution from a given  $y$  will be proportional to  $N$  or less than that. The contribution from each texture is smaller than a constant, and  $C^l$  increases as we go up in  $y$ , simply because there are more textures creating a r.m.s. fluctuation. Hence there will be a peak in  $C^l(y)$  at  $y : \Omega^s(y) \approx \Omega^{l(sat)}$ , and we may expect that most of the contribution to a given  $C^l$  will come from the scales where the filter starts to act. The contribution from these textures is of the order  $N\Omega^{l(sat)^2}$ , and recalling that  $N\Omega^s \approx const$ , we can expect a value of  $C^l$  proportional to  $\Omega^{l(sat)} \propto 1/l^2$ . This explains why we can always expect a roughly scale-invariant spectrum in the texture scenario. The only exception to this argument is the case where the  $\Omega^s > \Omega^{l(sat)}$  regime does not exist (or is irrelevant), simply because  $\Omega^{l(sat)}$  is greater than  $\langle \Omega_1 \rangle$ , the average angular size of the last texture. This is the case for low  $l$ , which do not act as a filter for any of the texture spots, because their cut-off scale is above the angular size of the last (and largest texture). Then, the largest contribution to  $C^l$  comes from the last texture, this being the case for all  $l : \Omega^{l(sat)} \gg \langle \Omega_1 \rangle$ . The last texture contribution to these  $C^l$  is, of course, independent of  $l$ , and proportional to  $\langle \Omega_1^2 \rangle$ . Hence we can expect a white noise type of spectrum ( $C^l \propto const$ ) in this  $l$  region. In practice, the transition from white noise to scale invariance happens very quickly. We never observe a white noise regime, but only a suppression for the low  $l$ .

This heuristic argument can be converted into an approximate formula by taking the toy-hat profile and carrying out explicitly the  $C^l$  integration, starting from  $y = \langle y_1 \rangle$ . Let us define  $l_1$  as

$$\Omega_1 = \Omega^s(\langle y_1 \rangle) = \frac{4\pi}{l_1(l_1 + 1)} \quad (43)$$



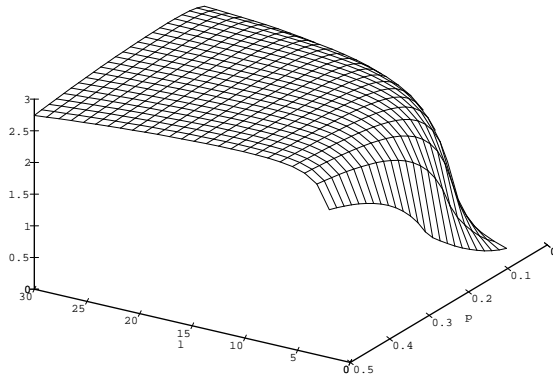


Figure 8: Approximate spectra  $l(l+1)C^l$  for various values of  $p_s$ .

(the  $l$ -scale of the last texture), and  $l_{ls}$  as

$$\Omega^s(y_{l_s}) = \frac{4\pi}{l_{ls}(l_{ls} + 1)} \quad (44)$$

(the  $l$ -scale of textures living at the last-scattering surface). Then

$$C^l \propto \int_{\Omega_{l_s}}^{\Omega_1} d\Omega \frac{W^{sl2}}{\Omega^{s2}} \propto \begin{cases} \Omega_1 - \Omega_{l_s} & \text{for } l \leq l_1 \\ 3\Omega^{l(sat)} - 2\frac{\Omega^{l(sat)2}}{\Omega_1} - \Omega^{ls} & \text{for } l \geq l_1 \end{cases} \quad (45)$$

giving mathematical expression to what we have said above. This leads to the approximate spectral formula

$$C^l \propto \begin{cases} \frac{1}{l_1(l_1+1)} - \frac{1}{l_{ls}(l_{ls}+1)} & \text{for } l \leq l_1 \\ \frac{3}{l(l+1)} - \frac{2l_1(l_1+1)}{(l(l+1))^2} - \frac{1}{l_{ls}(l_{ls}+1)} & \text{for } l \geq l_1 \end{cases} \quad (46)$$

with  $l_1 \approx 0.5/\tilde{p}_s$  and  $l_{ls} \approx 30/\tilde{p}_s$  for standard recombination, with  $\tilde{p}_s = 2\bar{p}_s$ . The approximate spectra were plotted in Fig. 8 with an arbitrary vertical scale. Confronting this with Fig. 4, we see that (46) does provide a good qualitative description of the spectra.

## 4 The two-point correlation function

The two-point correlation function  $C(\theta)$  is a tool sadly closer to experiment than the  $C^l$  spectrum (however see [14] for a more hopeful point of view). We will now show that  $C(\theta)$  is a very bad discriminator between inflationary and texture scenarios.  $C(\theta)$  is defined as

$$C(\theta) = \langle \frac{\delta T}{T}(\Omega) \frac{\delta T}{T}(\Omega') \rangle_{obs} \quad (47)$$

with  $\theta = (\widehat{\Omega}, \widehat{\Omega}')$ , ( $\Omega$  and  $\Omega'$  any two fixed directions in the sky). Making use of (17) this can be written as

$$C(\theta) = \sum_l C^l \frac{2l+1}{4\pi} P_l(\cos \theta). \quad (48)$$

The theoretical  $C(\theta)$  can be estimated from the sky average of  $\frac{\delta T}{T}(\Omega) \frac{\delta T}{T}(\Omega')$  with a fixed  $\theta = (\widehat{\Omega}, \widehat{\Omega}')$ :

$$C_{obs}(\theta) = \int \frac{d\Omega d\Omega'}{8\pi^2} \frac{\delta T}{T}(\Omega) \frac{\delta T}{T}(\Omega') \delta(\cos \theta - \cos(\widehat{\Omega}, \widehat{\Omega}')) \quad (49)$$

which after some algebra leads to

$$C_{obs}(\theta) = \sum_l C_l \frac{2l+1}{4\pi} P_l(\cos \theta) \quad (50)$$

with  $C_l$  defined as in (18). An expression for  $C(\theta)$  in texture scenarios can be found by replacing (22) in (48). It is curious that a simpler expression can be derived. Inverting the Legendre transform (15) one has

$$W^s(z, y) = \sum_l \frac{2l+1}{4\pi} W^{sl}(y) P_l(z). \quad (51)$$

If we define the Legendre-squared spot profile to be

$$W^{s(2)}(z, y) = \sum_l \frac{2l+1}{4\pi} W^{sl2}(y) P_l(z) \quad (52)$$

then the correlation function is simply

$$C(\theta) = \frac{\langle a^2 \rangle}{4\pi} \int_0^{y_{ts}} dy N(y) W^{s(2)}(\cos \theta, y). \quad (53)$$

The profile  $W^{s(2)}$  is the Legendre analogue of  $W^s \star W^s$  (where  $\star$  is the convolution) in Fourier analysis. Depending on whether the profiles are defined in the  $\theta$  or in the Legendre spaces it may be easier to use (53) or to combine (48) and (22). If one wants to take into account the telescope beam filtering, one should multiply the  $C^l$  in (48) by the square of the beam Legendre transform  $\mathcal{F}^{l2}$ . In the numerics we will use an approximation to the COBE beam  $\mathcal{F}^l = e^{-\frac{1}{2}(l+\frac{1}{2})^2 \sigma^2}$  with  $\sigma = 2\pi(10^\circ/360^\circ)$ .

We have also derived an expression for the cosmic variance in  $C_{obs}(\theta)$ . In Gaussian theories ([4] with a factor of 2 correction) we have:

$$\sigma_G^2(C_{obs}(\theta)) = \sum_l \sigma_G^2(C_l) \left( \frac{2l+1}{4\pi} \right)^2 P_l^2(\cos \theta) \quad (54)$$

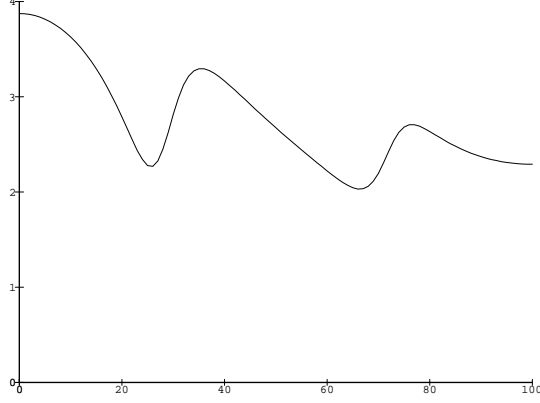


Figure 9:  $\epsilon(\theta)$  for Gaussian spots with ( $n = 1$ ,  $p_s = 0.25$ ).

with  $\sigma_G^2(C_l)$  given by (36). In the texture scenarios not only does one have to replace  $\sigma_G^2(C_l)$  by  $\sigma_{TX}^2(C_l)$  (as in (39)), but also terms in  $P_l P_{l'}$  (with  $l \neq l'$ ) appear, reflecting the inter- $l$  correlations. A rather elaborate calculation, in the moulds of Sec.3.3, brings us to

$$\sigma_{TX}^2(C_{obs}(\theta)) = \sum_{l'} V_{ll'} C^l C^{l'} \frac{2l+1}{4\pi} \frac{2l'+1}{4\pi} P_l(\cos \theta) P_{l'}(\cos \theta) \quad (55)$$

with

$$V_{ll'} = \frac{2\delta_{ll'}}{2l+1} + \left(1 + \frac{\sigma^2(a^2)}{\langle a^2 \rangle^2}\right) \frac{\int_0^{y_{ls}} dy N(y) W^{ls^2}(y) W^{l's^2}(y)}{(\int_0^{y_{ls}} dy N(y) W^{ls^2}(y)) (\int_0^{y_{l's}} dy N(y) W^{l's^2}(y))} \quad (56)$$

where, again, we have neglected terms in  $1/N_t$ . The intensity of the non-Gaussian correction to the cosmic variance can be measured by means of the quantity

$$\epsilon(\theta) = \frac{\sigma_{TX}^2(C_{obs}(\theta)) - \sigma_G^2(C_{obs}(\theta))}{\sigma_G^2(C_{obs}(\theta))} \quad (57)$$

which depends on  $n$ ,  $\bar{p}_s$ , and the profile. The dependence on  $n$  is trivial, so we define  $\tilde{\epsilon}(p_s, \theta) = \epsilon(n, p_s, \theta).n$ . The numerator in (57) can be rewritten as  $\langle (W^{s(2)})^2 \rangle$ , showing that the variance in  $C_{obs}(\theta)$  is always larger in texture scenarios than in similar Gaussian theories. As before, we adopt the attitude that while this does reduce the predictability of the theory on  $C(\theta)$ , it also signals non-Gaussian behaviour and the need of a non-Gaussian data-analysis approach to fully make out the predictions of the theory. In particular, on angular scales where  $\epsilon \gg 1$ , we know that it is worth studying the collapsed (to two points)  $n$ -point correlation function. In Fig. 9 we divided  $\theta \in (0, \pi)$  into 100 points and plotted  $\epsilon(\theta)$  for Gaussian spots with ( $n = 1$ ,  $p_s = 0.25$ ). The fact that the low  $l$  multipoles contribute to  $C(\theta)$  for all  $\theta$  distributes non-Gaussianity nearly uniformly over  $\theta$ . In Fig. 10 we analyse the various contributions to  $\sigma_{TX}^2$ , sep-

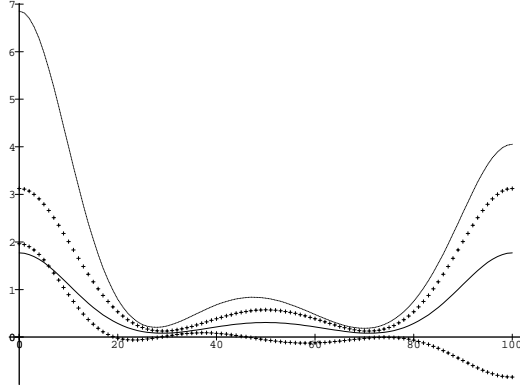


Figure 10:  $\sigma_{TX}^2$  (top line), and its Gaussian (bottom line), diagonal (top points), and off-diagonal (bottom points) in  $V_{ll'}$ , contributions.

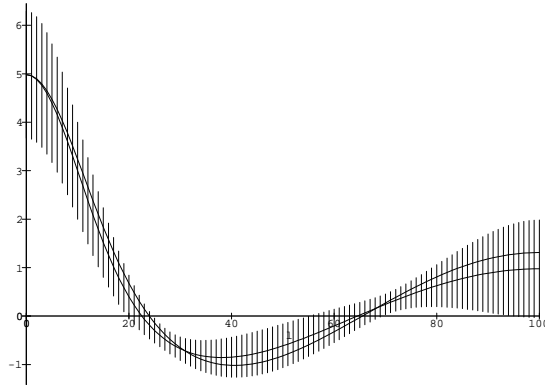


Figure 11:  $C(\theta)$  for Gaussian spots with ( $n = 1$ ,  $p_s = 0.25$ ) with its full cosmic variance error bars, confronted with its fitting  $n = 1.001$  theory (top line at  $C(\pi)$ ).

arating its Gaussian, diagonal and off-diagonal components in  $V_{ll'}$ . We note that the inter- $l$  correlations responsible for the off-diagonal elements of  $V_{ll'}$  can act so as to reduce the cosmic variance, an important fact which we shall make use of in [10]. Naturally, the subtle differences in the  $C^l$ -spectra pointed out at the end of Sec.3.4 are completely drowned in  $C(\theta)$ . As an example we have plotted in Fig. 11  $C(\theta)$  for the above texture theory, and for its fitting tilted spectrum inflationary theory. As  $C(\theta)$  spreads the low  $l$  over all  $\theta$ , the two theories come out completely confused. Note however that the normalization in the  $C^l$  and in  $C(\theta)$  can be substantially different (in Fig. 11 we used a different normalization procedure than in Fig. 7).

## 5 The last texture and non-Gaussianity at low $l$

In the derivation of (22) we made use of statistics for unordered textures. However, a similar expression could have been obtained using ordered textures. In this case one should be wary for the  $W_n^{sl}$  are not independent variables. Nevertheless formula (21) remains valid if one uses the marginal distribution functions of  $y_n$  in computing  $\langle W_n^{sl2} \rangle$  for each term in (21). The marginal distribution functions  $\bar{P}_n(y_n)$  are defined as

$$\bar{P}_n(y_n) = \int dy_1 \dots dy_{n-1} dy_{n+1} \dots dy_{N_t} P_{1 \dots N_t}(y_1, \dots, y_{N_t}) \quad (58)$$

and using (10) they can be found to be

$$\bar{P}_n(y_n) = N(y_n) e^{-M(y_n)} \frac{M^{n-1}(y_n)}{(n-1)!} \quad (59)$$

where  $M(y) = \int_0^y N(x) dx$ . Then:

$$C^l = \frac{\langle a^2 \rangle}{4\pi} \sum_{n=1}^{N_t} \int_0^{y_{i_s}} dy_n N(y_n) W^{ls2}(y_n) e^{-M(y_n)} \frac{M^{n-1}(y_n)}{(n-1)!} \quad (60)$$

and since  $N_t$  is very large we recover (22). The advantage of (60) is that it allows us to write

$$C^l = \sum_n C_n^l \quad (61)$$

with

$$C_n^l = \frac{\langle a^2 \rangle}{4\pi} \int_0^{y_{i_s}} dy_n N(y_n) W^{ls2}(y_n) e^{-M(y_n)} \frac{M^{n-1}(y_n)}{(n-1)!} \quad (62)$$

reporting the contribution of the  $n^{\text{th}}$  texture to the multipole  $C^l$ . In Figure 12 we plotted the  $C^{l*}$  spectrum for four plausible scenarios: for a Gaussian profile with  $p_s = 0.05$  and  $p_s = 0.1$  ( $n = 1$  in both cases), and for a SSSS profile with  $n = 0.25$  and  $n = 0.1$  ( $p_s = 0.2$  for both). Underneath the spectra we plotted the result of stopping the sum (61) at  $N_t$  from 1 to 10, thus obtaining the contribution of the first 10 textures to each  $C^l$ . In all the cases considered we notice that the low  $l$  multipoles are dominated by the contribution from the last texture. The  $l$  at which this stops being the case depends on the spot details (profile,  $n$ ,  $p_s$ ), but  $l = 2, 3$  always seem to be subject to this effect. Also the intensity of the last texture dominance at low  $l$  depends on the spot details, the effect being notably pronounced for Gaussian profiles with low  $p_s$ . As we go up in  $l$ , the last texture becomes less prominent, but no other single texture replaces it as a dominant feature. We may ask how many textures are responsible for, say, 95% of a given  $C^l$  for high  $l$ . Using the toy hat model and performing an approximate calculation

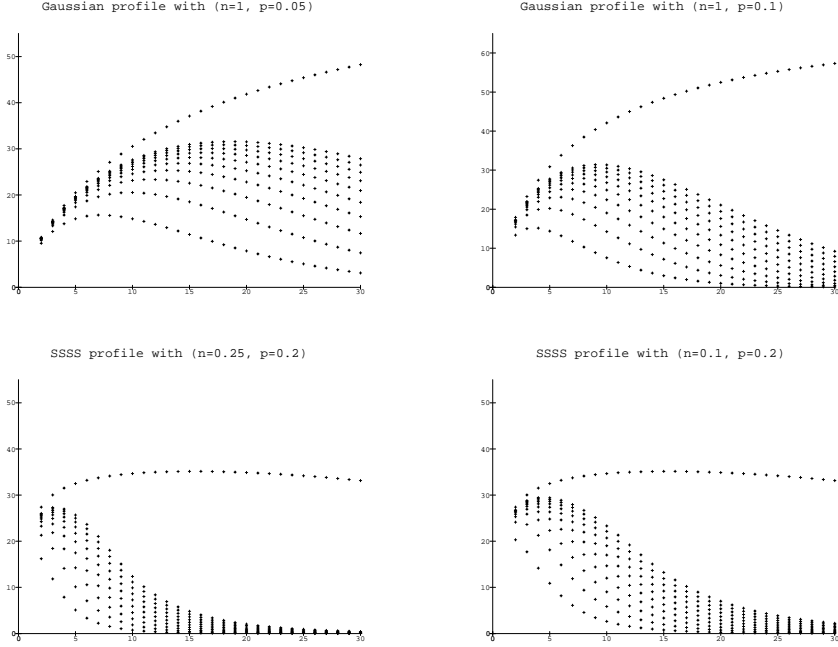


Figure 12: Contribution of the last ten textures for a Gaussian profile, with  $p_s = 0.05$  and  $p_s = 0.1$  ( $n = 1$  in both cases), and for a SSSS profile with  $n = 0.25$  and  $n = 0.1$  (and  $p_s = 0.2$ ).

similar to the one in Sec.3.5, we can show that this number is proportional to  $l^2$ . This implies that for high  $l$  the number of defects responsible for a given  $a_m^l$  is proportional to  $l$ .

These results have far reaching consequences. If one believes in flippant applications of the central limit theorem, then one can expect the  $a_m^l$  for high  $l < 30$  to be independent Gaussian distributed random variables, as they add up a large number of independent contributions (proportional to  $l$ ). We have now shown that this argument can certainly not be repeated for the low  $l$ . In fact, our remark in Sec.3.3 that  $\sigma_{TX}^2(C_l) > \sigma_{Gauss}^2(C_l)$ , and the numerical results plotted in Fig. 3, *prove* that the  $a_m^l$  are distinctly non-Gaussian at low  $l$ . This also implies that these  $a_m^l$  are dependent random variables [11]. We can now understand better why this is so. The non-Gaussian features in the  $a_m^l$  for low  $l$  result from the fact that they are mostly due to one single lumpy object blatantly different from Gaussian noise. We may even expect the  $a_m^l$  for low  $l$  to reproduce the morphology, size, and other features of the last defect. Devising a data-analysis method capable of uncovering these features is the purpose of [10]. We should stress that both the central limit theorem and Fig. 3 strongly suggest, but still do not prove, that the  $a_m^l$  are Gaussian for high  $l < 30$ .

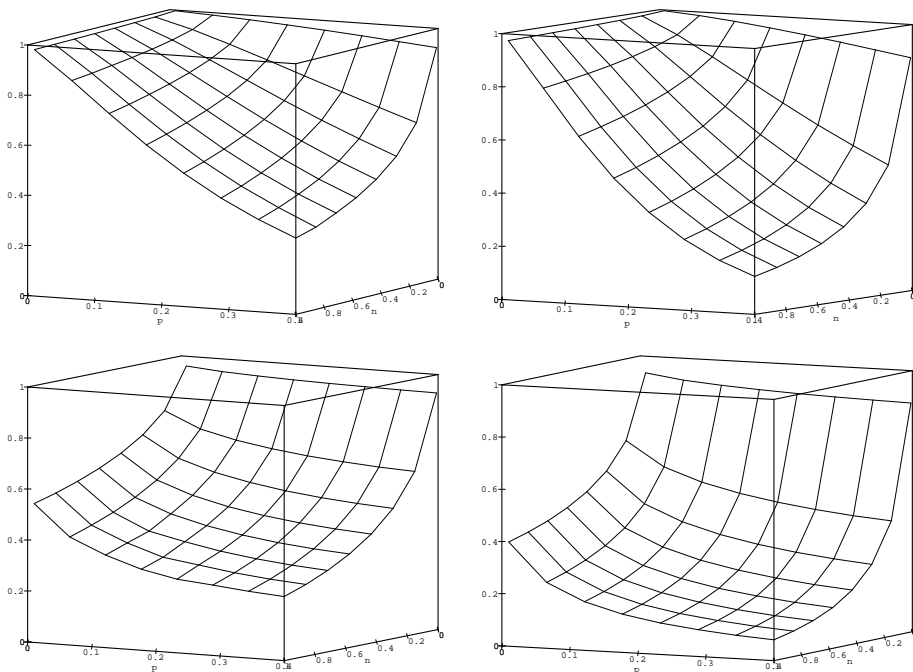


Figure 13: The  $\alpha^2$  and  $\alpha^3$  function for a Gaussian (top), and a SSSS profile (bottom).

The non-Gaussian toy model studied in [11] showed in which way the low  $l$  multipoles would display non-Gaussian behaviour if they were fully due to the last texture. The contribution from  $n > 1$  textures will soften this non-Gaussianity. Hence a plausible measure for the expected non-Gaussianity present in a low  $l$  multipole is  $\alpha^l = C_1^l / C^l$ , a quantity which depends on the profile,  $n$ , and  $p_s$ . We have computed numerically  $\alpha^2$  and  $\alpha^3$  for a Gaussian and a SSSS profile. The results are plotted in Fig. 13. A better connection between  $\alpha^l$  and detailed features of non-Gaussianity measure distribution functions will be given in [10].

## 6 What's new?

The focus in this paper was to derive for texture scenarios whatever one normally derives for Gaussian theories ( $C^l$ ,  $C(\theta)$ , and their cosmic variances). We met anomalous behaviour (eg. formulae (39) and (55)) which (theoretically) indicates non-Gaussianity, but we have left to the sequels [10] and [15] the task of developing a non-Gaussian data analysis method. On the whole, within the standard lore, the results obtained are surprisingly similar to inflationary scenarios. Still, we found a few novelties. We discovered that texture spectra are tilted, but

not uniformly. Fitting a tilted spectrum for  $l \in (25, 30)$  (see Fig. 6) leaves a significant suppression of power at low  $l \in (2, 5)$  (see Fig. 7). We have also computed directly the cosmic variance error bars in  $C_l$  and  $C_{obs}(\theta)$ , and found them to be larger than in comparable Gaussian theories (see formulae (39) and (55) and Figs. 3 and 10). In fact, if the non-Gaussian correction is very large (which does happen for most of the parameter values suggested in the literature), cosmic variance drowns the otherwise  $1\text{-}\sigma$  suppression of power at low  $l$  mentioned above (see Fig. 7). However, one should not give way to despair. Large non-Gaussian corrections to cosmic variance only hint that we have not applied to the theory the right data analysis procedure. To give a flavour of [15] let us point out that as the  $C_l$  are dependent random variables in non-Gaussian theories ([11]), it may happen that *the  $C_l$  spectrum shape seen by any observer is never the average  $C^l$  spectrum shape*. A more intelligent method to make predictions on  $C_l$  spectra and to estimate global parameters in the  $C^l$  spectrum is in order. It appears that even a proper study of the  $C^l$  (or  $C_l$ ) spectrum for textures requires non-Gaussian data analysis.

The central result in this paper is undoubtedly the *proof* that texture low  $l$  multipoles are strongly non-Gaussian, and that the last texture is to be blamed for this (see Sec.5). We showed how the low  $C^l$  are mostly due to the last texture (slightly perturbed by the one after - see Fig. 12), and so we may expect the last texture's non-Gaussian features to be imparted on the low  $l$  multipoles. In [11] we proposed the use of  $m$ -structure and inter- $l$  measures to complement the  $C^l$ .  $m$ -structure measures act as multipole shape factors. Inter- $l$  measures correlate preferred directions in two multipoles. These two types of quantities are uniformly distributed in Gaussian theories. In topological defect scenarios we can expect low  $l$  shape factors to reflect the morphology of the last defect. Hence their distributions should be non uniform, peaking at different values for, say, texture and cosmic strings. Inter- $l$  measures should also display the correlations between the various low  $l$  which are all due to the same last defect. It remains to be seen ([10]) how much cosmic confusion there is between these signals and their Gaussian counterparts.

On a lower key this paper was simply intended as an analytical model for texture CMBR skies with the greatest possible generality. We tried to leave as free parameters whatever simulations have failed to determine. The point is to find out what exactly must be decided in order to answer a particular question. We have concluded, for instance, that the  $C^l$  spectrum shape is insensitive to  $n$  or  $a$ , and depends very little on the spots' profile, once the identifications (33) and (35) have been made. The controlling parameter is  $\bar{p}_s$  which fixes the spectrum tilt at intermediate  $l$  (see Fig. 6). The spectrum normalization, on the other hand, depends on all the parameters of the model (see Sec.3.1), which must be evaluated before any prediction for the texture symmetry breaking energy or bias parameter can be made. Interestingly enough, we found that the low  $l$  non-Gaussianity effects depend only on  $n$ ,  $\bar{p}_s$ , and profile (Sec.5). These are not free



parameters of the theory, so one ought to decide on this important issue purely by means of hard work.

The paradigm proposed here cannot easily be adapted to cosmic string scenarios. Neglecting non-circular spot modes is, in texture scenarios, only slightly inaccurate. The string counterpart to circular spots, line discontinuities cut-off at horizon distance (as in [16]), is definitely a much cruder approximation. More importantly, neglecting texture spot-spot correlations introduces only a small error (in fact it would not be difficult to incorporate small correlations in our model). On the contrary, the various segments of the string network form a Brownian random walk. Segments linked to each other are therefore very highly correlated, making an analytical treatment cumbersome. Uncorrelated string segments (as in [16]) are not very realistic. Overall, although we can boast a more realistic set of assumptions than [16], this is mostly due to the fact that textures are far simpler than strings. This also justifies why we can go further than [16]. We treated with greater rigour (no “ergodic” assumptions) a much broader set of models. We also managed to treat exactly (within the model) the problem of cosmic variance. Finally, greater sophistication in the statistical machinery opened doors to the issue of non-Gaussian data analysis in defect scenarios (developed further in [10, 15]).

## Acknowledgments

I would like to thank N.Turok and P.Ferreira for discussion in connection with this paper, and K.Baskerville for help in its preparation. This work was supported by a fellowship at St.John’s College, Cambridge.

## References

- [1] M.White, D.Scott, and J.Silk, *Am.Rv.Astron.Astrophys.* 32 (1994) 319.
- [2] U.Pen, D.Spergel, and N.Turok, *Phys.Rev.* D49 (1994) 692.
- [3] B.Allen, R.Caldwell, P.Shellard, A.Stebbins, and S.Veeraraghaven, Cosmic strings confront COBE, in *Birth of the Universe*, F. Occhiniero (ed), Rome 1994.
- [4] J.Bond and G.Efstathiou, *MNRAS* 226 (1987) 655.
- [5] P.Coles, *MNRAS* 234 (1988) 509.
- [6] R.Scaramella and N.Vittorio, *MNRAS* 263 (1993) L17.
- [7] T.Falk, R.Rangaranjan, and M.Srednicky, *Ap.J.Lett.* 403 (1993) L1.

- [8] J.Borrill, E.Copeland, A.Liddle, A.Stebbins, and S.Veeraraghaven, Phys.Rev. D50 (1994) 2469.
- [9] R.Durrer, A.Howard, and Z.Zhou, Phys.Rev. D49 (1994) 681.
- [10] J.Magueijo, The last texture: a large angle CMBR non-Gaussian signal, in preparation.
- [11] J.Magueijo, Phys.Lett.B 342 (1995) 32.
- [12] R.Durrer, Phys.Rev. D42 (1990) 2533.
- [13] A.Stebbins and S.Veeraraghaven, Phys.Rev. D51 (1995) 1465.
- [14] D.Scott, CMB anisotropies: an overview, Report CfPA-95-TH-03.
- [15] J.Magueijo, Non-Gaussian CMBR angular power spectra, Report DAMTP-95-18.
- [16] L.Perivolaropoulos, Phys.Lett.B 298 (1993) 305; Phys.Rev.D48 (1993) 1530.